

I. Ngounouno · B. Déruelle · D. Demaiffe · R. Montigny

Petrology of the Cenozoic volcanism in the Upper Benue valley, northern Cameroon (Central Africa)

Received: 16 June 2002 / Accepted: 2 December 2002 / Published online: 24 January 2003
© Springer-Verlag 2003

Abstract Thirty-one plugs of alkaline volcanic rocks of Cenozoic age (37 Ma in mean) occur in the Upper Benue valley, northern Cameroon (Central Africa). The complete alkaline series (alkaline basalts, hawaiites, mugearites, phonolites, trachytes and rhyolites) is represented. Basalts contain phenocrysts of olivine, Al-Ti-rich diopside, and Ti-magnetite, and hawaiites-abundant microphenocrysts of plagioclase. Mugearites have a trachytic texture and contain xenocrysts of K-feldspar, apatite, quartz and unstable biotite. Phonolites are peralkaline. Trachytes (peralkaline and non-peralkaline) and rhyolites are characterised by their sodic mineralogy with aegirine-augite, richterite, and arfvedsonite phenocrysts. There is a large compositional gap between basaltic and felsic lavas, except the mugearites. Despite this gap, major- and trace-element distributions are in favour of a co-magmatic origin for the basaltic and felsic lavas. The Upper Benue valley basalts are similar in their chemical

and isotopic features to other basalts from both the continental and oceanic sectors of the Cameroon Line. The Upper Benue valley basaltic magmas ($^{87}\text{Sr}/^{86}\text{Sr} \approx 0.7035$; $\varepsilon \text{Nd} = +3.9$) originate from an infra-lithospheric reservoir. The Sr–Nd isotopic composition and high Sr contents of the mugearites suggest that they are related to mantle-derived magmas and that they result from the mixing, at shallow crustal levels, of a large fraction of trachytic magma with a minor amount of basaltic magma. Major-element modelling of the basalt–trachyte evolution (through hawaiite and mugearite compositions) does not support an evolution through fractional crystallization alone. The fluids have played a significant role in the felsic lavas genesis, as attested by the occurrence of F-rich minerals, calcite and analcite. An origin of the Upper Benue valley rhyolitic magmas by fractional crystallization of mantle-derived primitive magmas of basaltic composition, promoted or accompanied by volatile, halogen-rich fluid phases, may be the best hypothesis for the genesis of these lavas. These fluids also interact with the continental crust, resulting in the high Sr-isotope initial ratios (0.710) in the rhyolites, whereas the Nd isotopic composition has been less affected ($\varepsilon \text{Nd} = +0.4$).

Electronic Supplementary Material Supplementary material is available for this article if you access the article at <http://dx.doi.org/10.1007/s00410-002-0438-6>. A link in the frame on the left on that page takes you directly to the supplementary material.

I. Ngounouno
Département des Sciences de la Terre, Faculté des Sciences,
Université de Ngaoundéré, B.P. 454, Ngaoundéré, Cameroun

B. Déruelle (✉)
Laboratoire de Magmatologie et Géochimie Inorganique
et Expérimentale, CNRSESA 7047, IUFM Académie de Versailles,
Université Pierre et Marie Curie, 4 Place Jussieu,
75252, Paris cedex 05, France
E-mail: deruelle@ccr.jussieu.fr

D. Demaiffe
Laboratoire de Géochimie Isotopique,
Université Libre de Bruxelles, 50 Avenue F.D. Roosevelt,
C.P. 160/02, 1050, Bruxelles, Belgique

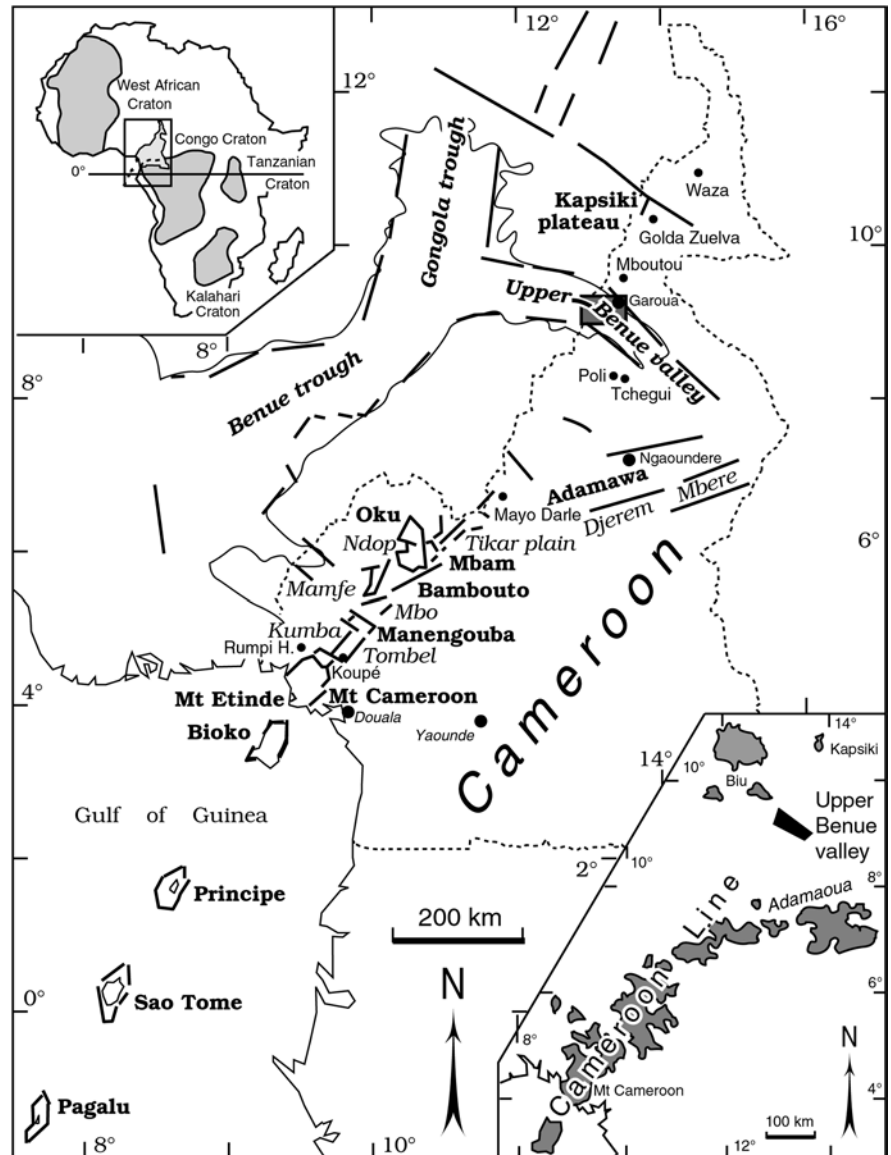
R. Montigny
École et Observatoire de Physique du Globe,
UMR CNRS 7516, Université Louis Pasteur,
5 Rue Descartes, 67100, Strasbourg, France

Editorial responsibility: J. Touret

Introduction

The Benue trough (Fig. 1) is an intra-continental rift trending N50°E and belonging to the Mid-African Rift System (MARS). The MARS propagates far inside Africa from the earlier equatorial rifts of the South Atlantic (Kampunzu and Popoff 1991; Guiraud and Bosworth 1997). The Benue trough extends northwards into the Gongola branch and eastwards into the Yola branch (Nigerian part of the Upper Benue valley). The Garoua rift is the N120°E–130°E propagation in Cameroon of the Yola branch and is limited by strike-slip faults. The main stage of rifting occurred during Neocomian to Lower Aptian times (Benkhelil 1988). Then, subsidence during the Aptian and Albian favours the accumulation

Fig. 1 Location of the study area (*shaded rectangle*) in the Upper Benue valley. The Cameroon Line, a succession of horsts and rifts (rift names in *italic*), the Adamawa horst, the Djérem Mbéré rift, and the main volcanic and plutonic complexes are also indicated (after Déruelle et al. 1991). African cratons are after Kampunzu and Popoff (1991)



of voluminous conglomerates and sandstones (up to 5,000 m thick) which were folded during a regional Santonian compression (Guiraud 1993; Ngounouno et al. 1997) and faulted during Cenozoic times.

Numerous interpretations have been given to explain the formation of the Cameroon Line (for a comprehensive review, see Déruelle et al. 1991). Among these, the Cameroon Line has been considered as:

- a volcanic alignment made of a succession of horsts and grabens (Gèze 1943; Déruelle et al. 1987, 1991);
- a volcanic and subvolcanic alignment resulting from hot-spot activity (Duncan 1981; Morgan 1983; Van Houten 1983);
- an active rift system produced by a thermal anomaly in the asthenosphere, this last model being essentially based upon the approximate "Y" shape and similar size of both the Benue trough and the continental

segment of the Cameroon Line–Adamawa horst–Biu Plateau (Fitton 1980, 1983).

All the above interpretations have been recently discussed (Déruelle et al. 1991), and the most widely accepted structural explanation is that the N30°E Cameroon Line is due to the rejuvenation of a Pan-African N70°E fracture zone at the beginning of the opening of the Atlantic Ocean (Moreau et al. 1987). More recently, the Cameroon Line has been distinguished from a rift system, and it is considered as a "hotline" resulting from lithospheric cracks (N30°E) tapping sublithospheric mantle (Déruelle et al. 1998). The mantle hotline hypothesis has been supported by deep-imaging seismic and gravity study on offshore Cameroon Line (Meyers et al. 1998) and recent geochemical study on Bambouto, Oku and Adamawa (Marzoli et al. 1999, 2000). Whether or not the volcanism of the Cretaceous Garoua rift is related to that of the

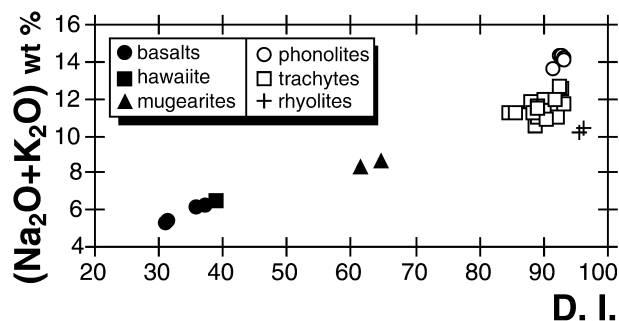


Fig. 3 Nomenclature of the lavas of the Upper Benue valley according to their differentiation index (D.I., Thornton and Tuttle 1960; see Table 3)

lava blocks. Sometimes, the blocks are left above sandstone erosion columns. The sandstones are slightly metamorphosed (on a metric scale) into reddish quartzites at the contact with felsic lavas. The total volume of exposed lavas is around 5.3 km³. Felsic lavas (4.6 km³ exposed) and the mugearites (0.7 km³ exposed) are by far more voluminous than basaltic ones (0.001 km³ exposed). A theralite dyke outcrops at Nakong. This rock contains small phenocrysts of olivine (16 vol%), diopside (10 vol%) and kaersutite (5 vol%) enclosed by plagioclase oikocrysts. Analcite is abundant. Numerous dykes of lamprophyres (monchiquites) of Cenozoic age (37.5 ± 2.3 Ma) outcrop in the Tchircotché area. They are composed of diopside and subsilicic kaersutite phenocrysts, Ba-Ti-rich biotite microphenocrysts, and Cr-diopside xenocrysts scattered in a matrix of analcitic composition containing oligoclase, albite and sanidine-anorthoclase microlites and carbonate ocelli.

Well-defined lineaments have been reported on the geological map. They correspond to the main directions formerly recognised along the Cameroon Line (N–S, N70°E, E–W and N130°E; Moreau et al. 1987). These directions, which are also recognised in the surrounding Precambrian basement, correspond to crust discontinuities inherited from the Pan-African orogeny and reactivated during Mesozoic and Cenozoic times.

K–Ar ages

The analytical procedure which is fully described elsewhere (Bonhomme et al. 1975; Montigny et al. 1988) is summarised below. Potassium content is determined by flame photometry with a lithium internal standard. Argon is extracted in a heat-resistant glass vacuum apparatus and determined by isotope dilution (³⁸Ar

as a tracer), using a MS20 mass spectrometer. All samples are measured in the static mode. The set of constants recommended by Steiger and Jäger (1977) is used for age calculation. Quoted uncertainties represent estimates of analytical precision at one standard deviation. They are calculated after the procedure given by Cox and Dalrymple (1967).

The striking feature of the analytical results (Table 1) is an age convergence around 37 Ma. Irrespective of rock type, five samples give this date and the slightly different values yielded by basalts 4P and G22, 39.7 ± 0.9 and 34.8 ± 0.8 Ma respectively, cannot be considered to be significantly different. The assumed instantaneous cooling of the rocks, the freshness of the samples and the aforementioned age convergence lead us to regard the 37-Ma age as mirroring the emplacement of the volcanic rocks. Moreover, the age range suggests a rather discrete event between 35 and 40 Ma.

Nomenclature and petrography

The lavas are named (Fig. 3) according to both the differentiation index (D.I., Thornton and Tuttle 1960) and phenocryst distribution (Fig. 4, Table 2). Basaltic lavas include basalts and hawaiites. Felsic lavas are phonolites, trachytes, and rhyolites. Mugearites are intermediate lavas between the basaltic and felsic groups.

Basalts (4P, G23, G22 and T1) have a porphyritic texture with phenocrysts of olivine (0.6 to 2 mm), brown clinopyroxene (no green cores have been observed), Fe–Ti oxides and rare plagioclase. The groundmass is fine-grained with an intergranular texture, and composed of plagioclase microlites, subhedral to anhedral brown clinopyroxene and Fe–Ti oxides. Analcite of hydrothermal origin (<150 μm) crystallised lately between plagioclase laths. Basalt 4P contains xenocrysts of olivine (with Cr-rich spinel inclusions of ≈20 μm) and quartz (2 to 5 mm). The quartz xenocrysts are embayed and rimmed by brown glass and surrounded by a green clinopyroxene corona; some have completely recrystallised into small crystals of clinopyroxene.

The hawaiite (sample K98) contains abundant plagioclase microphenocrysts (up to 0.5 mm) and scarce phenocrysts of clinopyroxene (with pink core and brownish rim) and of Fe–Ti oxides. The groundmass is rich in plagioclase, granular clinopyroxene, biotite (<0.1 mm) and Fe–Ti oxides (10–30 μm).

Mugearites (samples BG1, BG3) have a trachytic texture. They are distinct from basaltic lavas as they do not contain any of the phenocrysts present in these lavas. They contain xenocrysts of K-feldspar (sometimes replaced by carbonates and analcite), apatite, and unstable biotite more or less transformed into Fe–Ti oxides

Table 1 Whole-rock K–Ar analytical results for the Upper Benue valley lavas ($\lambda_e = 0.581 \times 10^{-10} \text{ a}^{-1}$; $\lambda_\beta = 4.962 \times 10^{-10} \text{ a}^{-1}$; $^{40}\text{K}/\text{K} = 1.167 \times 10^{-4} \text{ mol/mol}$)

Sample number, petrographic type	K ₂ O (wt%)	100 $\frac{\text{rad. } ^{40}\text{Ar}}{\text{total } ^{40}\text{Ar}}$	Rad. ⁴⁰ Ar (10 ⁻¹¹ mol/g)	Age (± σ) (Ma)
G22, basalt	2.05	84	10.39	34.8 ± 0.8
4P, basalt	1.33	67	7.69	39.7 ± 0.9
4E, trachyte	5.36	89	29.24	37.5 ± 0.6
MU1, trachyte	5.41	77	29.41	37.4 ± 0.6
F2, rhyolite	4.32	34	23.11	36.8 ± 0.9
4L, trachyte	5.33	91	28.93	37.3 ± 0.6

Fig. 4 Distribution of minerals in Upper Benue valley lava series according to the D.I. of the lavas (see Table 3)

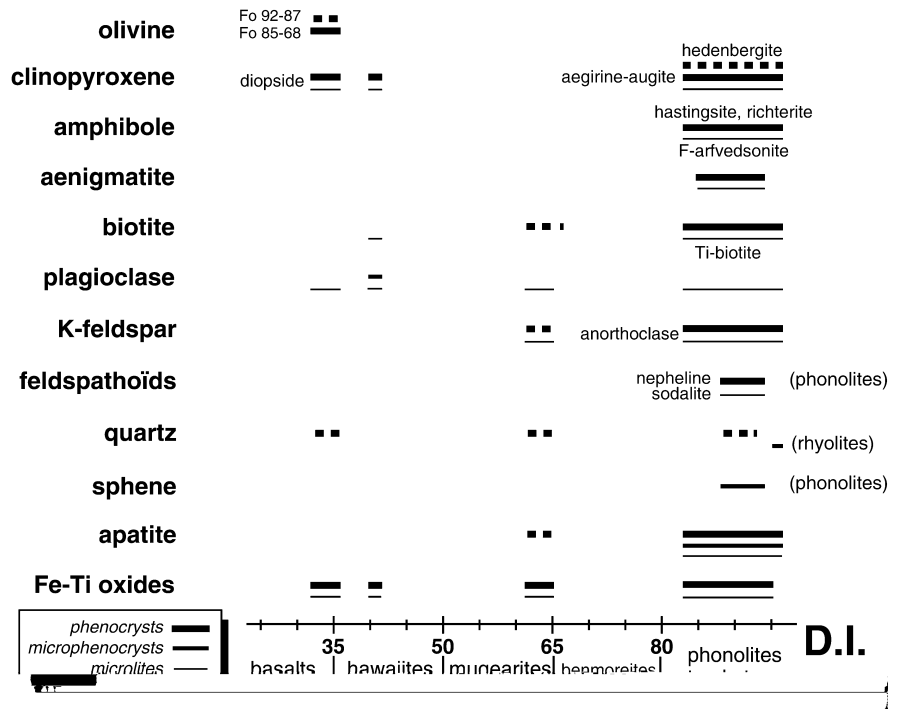


Table 2 Modes of Upper Benue valley lavas (in vol%) determined by counting 3,500 points

Lava type	Basalt			Hawaiite		Mugearite			Phonolite			Trachyte						Rhyolite		
	4P	G23	T1	K98	BG3	R4	N6	G5	F9	R112	4G	R6	4L	F5	4E	MD5	KA4		MU1	F3
Phenocrysts																				
Quartz																				0.4 ^a
K-feldspar							3.2	6.3	11.1	9.9	4.6	1.3	7.8	1.2	5.2	3.7	0.5	30.2	18.8	
Ca-plagioclase	0.2	<0.1	<0.1	5.1 ^a																
Albite							3.8	3.4	36.3								0.5	4.1		
Nepheline							13.3	6.3	0.6											
Olivine	10.5	10.4	2.2																	
Clinopyroxene	0.6	6.5	1.7	0.1			2.1	2.4										1.6	2.7	0.6
Amphibole									0.6											
Aenigmatite							1.3													
Biotite										4.3	2.2	0.1	0.2	2.2	0.6	1.3	1.1			
Fe-Ti oxides	2.1	7.1	0.9	1.3	5.1			0.3	0.6	1.6	1.0	1.3	1.1	1.5	0.6				0.8	
Apatite							0.1			1.3	1.9	1.2	0.3	0.6	0.1	0.9	0.1			
Total	13.4	24.0	4.8	6.5	5.1		23.8	18.7	38.1	18.3	15.0	7.2	3.8	13.2	2.7	14.5	4.9	10.2	49.2	21.4
Groundmass	81.2	69.8	87.6	93.5	84.5		75.2	81.3	61.9	81.7	85.0	92.8	96.2	86.8	97.3	85.5	95.1	89.8	50.8	78.6
Xenocrysts																				
Quartz	2.4	4.4	6.5		1.4															
K-feldspar					4.7															
Olivine	1.0																			
Clinopyroxene	2.0	1.8	1.1				1.0	<0.1												
Biotite					4.2															
Apatite					0.1															

^aMicrophenocrysts (diameter between 0.05 and 0.5 mm)

and chlorite. The matrix is made of microlites of K-feldspar and Fe-Ti oxides and of scarce laths of plagioclase (0.1–0.2 mm long). Round-shaped xenocrysts of quartz (3 to 5 mm diameter) can occasionally be present.

Phonolites are peralkaline ($1.01 < P.I. < 1.07$) with normative acmite (up to 1.15%) and Na-silicate. The texture is trachytic with hedenbergite, aegirine-augite and aenigmatite phenocrysts surrounded by small, aligned albite and sanidine microlites stacked upon one

another. Nepheline occurs as large phenocrysts and is often replaced by analcite. Hastingsite phenocrysts partially transformed into tiny Fe–Ti oxides and sodic hedenbergite are present in some phonolites (B2 and G5) which can therefore be distinguished from the others. Microphenocrysts of sodalite are observed around rounded albite phenocrysts (R4, N6). Spinel and apatite microphenocrysts are commonly present. Sieve-textured crystals of plagioclase are common, with a limpid core surrounded by a dark zone made of an inhomogeneous mixture of skeletal plagioclase and glass. Xenocrysts (up to 6 mm long) of Ca-rich clinopyroxene are commonly observed (sample R4).

Trachytes and rhyolites are characterised by their sodic mineralogy with aegirine-augite, richterite, and arfvedsonite phenocrysts. Trachytes do not contain quartz microphenocrysts whereas these are ubiquitous in rhyolites. Some trachytes are almost aphyric whereas others are highly porphyritic (up to 49 vol% phenocrysts), with anorthoclase as the dominant phenocryst phase. The matrix of trachytes is composed of flow-aligned alkali feldspar, richterite, biotite, apatite, and Fe–Ti-oxide microlites. Analcite is interstitial and quartz xenocrysts may occur.

Two types of trachytes occur (peralkaline and non-peralkaline), independently of their quartz-normative content.

Peralkaline trachytes (MU1, KA4) contain phenocrysts of aegirine-augite, richterite, arfvedsonite, aenigmatite, albite and sanidine–anorthoclase. Aegirine-augite crystals are sometimes pseudomorphosed by magnetite. Peralkaline trachytes have normative acmite (up to 1.7%) and Na-silicate, and their P.I. is comprised between 1.0 and 1.1.

Non-peralkaline trachytes can be classified into two quartz-normative groups. Trachytes from both groups have neither acmite nor Na-silicate in their norms, and their P.I. is lower than one. All contain phenocrysts of anorthoclase rimmed by sanidine. Biotite-richterite-bearing trachytes (4G, MD4, R6, 4L, DJ1, F5, 4E, MD5) are distinct from biotite-bearing trachytes (B8, F7, F9, F10, R111, R112). The former contain phenocrysts and microlites of arfvedsonite or richterite; the phenocrysts of biotite and richterite are sometimes replaced by carbonates. The latter contain phenocrysts of Fe–Ti oxides.

The rhyolites (F2, F3) contain quartz and alkali amphibole microphenocrysts (<0.6 mm), aegirine-augite and anorthoclase phenocrysts. They have a microlitic porphyritic texture and are peralkaline, with normative acmite (up to 0.8%) and Na-silicate, and high P.I. (≈ 1.1). The matrix is made of aegirine-augite (<0.2 mm) and arfvedsonite microphenocrysts, and late analcite and calcite.

Mineralogy

All mineral analyses were performed on an automated SX Cameca electron microprobe at the University Pierre et Marie Curie, Paris

(Ngounouno 1993; eTables 1 to 8; note that eTables can be found in the electronic supplementary material). They display evolutionary compositional trends according to increasing differentiation of their host lavas.

Olivine

Mg-rich olivine (eTable 1) occurs only in basalts and is often the dominant phenocryst phase. The crystals are generally homogeneous, but can sometimes have Mg-rich cores (Fo_{83-71}) and less magnesian rims (Fo_{72-68}). Crystallisation temperatures for phenocrysts have been estimated at $1,150 \pm 20$ °C (after Roeder and Emslie 1970, and Leeman 1978, using bulk-rock composition as a liquid).

Clinopyroxenes

Ca-rich pyroxene occurs in basalts and hawaiites (eTable 2). Compositions range from $\text{Wo}_{48}\text{En}_{38}\text{Fs}_{14}$ to $\text{Wo}_{45}\text{En}_{43}\text{Fs}_{12}$ and belong to the diopside field of the pyroxene quadrilateral (not shown). The phenocrysts are rich in aluminum (3.3–7.2 wt% Al_2O_3) and titanium (1.8–4.8 wt% TiO_2), the highest Al and Ti contents being found in rims. Ti/Al ratios are almost constant (0.32 to 0.35) in cores and rims. Assuming a temperature of 1,000 °C, equilibrium pressures can be estimated at 2.7 ± 0.4 kbar (after Nimis 1999) for the cores of phenocrysts in basalts. In phonolites, peralkaline trachytes and rhyolites, pyroxene phenocrysts and microlites display a large compositional range (Fig. 5), from sodic hedenbergite to aegirine. Their Na, Fe^{3+} , and Ti contents increase with decreasing Ca and Mg contents. High TiO_2 contents (3.4 wt%) in aegirine microlites indicate a low-crystallisation temperature (<600 °C; Ferguson 1977). The occurrence of Fe–NAT ($\text{NaTi}_{0.5}\text{Fe}^{2+}_{0.5}\text{Si}_2\text{O}_6$) in aegirine microlite rims suggests low oxygen fugacity during crystallisation (Nielsen 1979; Duggan 1988).

Amphiboles

Hastingsite, richterite and arfvedsonite occur in phonolites, trachytes and rhyolites (Fig. 6; Table 3). Cores of hastingsite

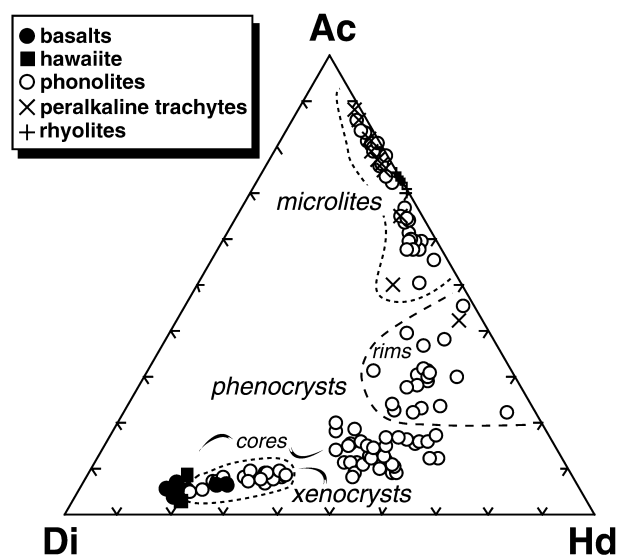


Fig. 5 Compositional variations of the pyroxene phenocrysts and microlites from the Upper Benue valley felsic lavas in the Di–Hd–Ac diagram (diopside–hedenbergite–acmite, cation%; nomenclature after Morimoto 1989). Phenocrysts from basalts and hawaiite, and xenocrysts from basalts and phonolite R4 are also indicated

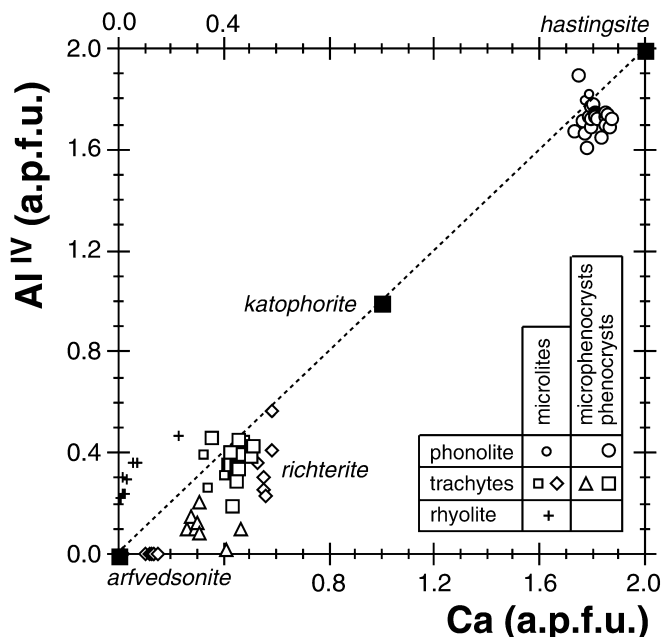


Fig. 6 Alkali amphiboles from the Upper Benue valley felsic lavas. Atoms per formula unit (a.p.f.u.) are calculated after Leake et al. (1997). Theoretical end-member compositions of hastingsite, katophorite and arfvedsonite (Ernst 1962) are indicated by closed squares

phenocrysts are richer in Mg, Ti, and Ca, and poorer in Fe and Na than rims. Richterite occurs as subhedral phenocrysts and as microlites. Phenocrysts are zoned with Al-Mg- and Fe-Mn-poor cores. Richterite is characterised by a wide range in Mg# (0.10–0.23), high alkali ($(\text{Na}_2\text{O} + \text{K}_2\text{O}) > 8.0$ wt%) and FeO contents (up to 33.9 wt%), moderate TiO_2 (0.2 to 1.6 wt%), and low Al_2O_3 (0.2 to 1.7 wt%) contents. Al–Ti substitution occurs at low levels (less than 0.2 atom per formula unit). Iron occurs as Fe^{2+} . Arfvedsonite is rich in Mg (up to 3.6 wt% MgO), poor in Al (<0.4 wt% Al_2O_3) and Ca (0.7–1.4 wt% CaO), and contains unusually large amounts of Mn (up to 7.3 wt% MnO) and F (up to 4.6 wt%). Such high Mn contents could result from low oxygen fugacities which prevent Fe–Ti-oxide crystallisation in the peralkaline trachytes and rhyolites. In peralkaline trachytes, the high Fe contents in richterite indicate temperatures around 950 °C, oxygen fugacities equivalent to the FMQ buffer, and low pressure during crystallisation (Charles 1975). Nevertheless, high F contents in richterite and arfvedsonite indicate crystallisation under low oxygen fugacity in a late magmatic-subsolidus stage (Strong and Taylor 1984). Amphibole compositions vary in the peralkaline felsic lavas (Fig. 6) from hastingsite to richterite and arfvedsonite, involving dominantly substitutions under reducing conditions according to the $\text{Al}^{\text{IV}} \leftrightarrow \text{Ca}$ substitution. We refer to this evolution from hastingsite and richterite (igneous) to arfvedsonite (oikocrystic amphiboles) as the subsolidus trend (Giret et al. 1980).

Biotite

Biotite phenocrysts (eTable 4) and microlites occur in trachytes. They are rich in Fe (Mg/Fe = 1.1–1.7), Ba (up to 6.2 wt% BaO), Al (≈ 13.5 wt% Al_2O_3) and Ti (up to 8.5 wt% TiO_2 , Fig. 7). Occurrence of Fe^{3+} is expected in the tetrahedral site, as Si and Al are not sufficient to fill this site ($\text{Si} + \text{Al} < 7.9$), and the number of cations in Y-sites is below the theoretical value (6). Fluorine contents are high (up to 2.4 wt%). High Ti contents in biotite indicate high temperature (1,000 °C, estimate after Hansen 1980), high oxygen fugacity, and low pressure (estimates after Esperança and Holloway 1987) during crystallisation.

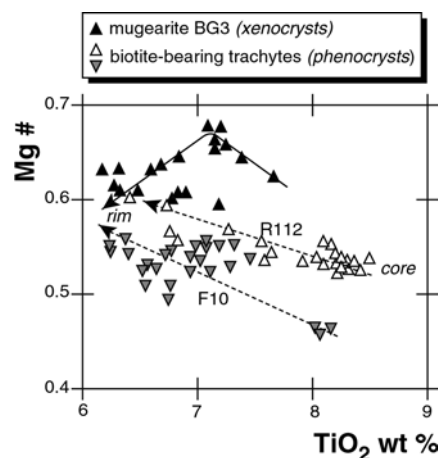


Fig. 7 Compositional variations of the biotite from the Upper Benue valley lavas in the TiO_2 –Mg# diagram. Arrows indicate the core to rim zonation of the phenocryst or xenocryst

Aenigmatite

Phenocrysts and microlites of aenigmatite (eTable 5) occur in peralkaline trachytes and in some phonolites. Aenigmatite phenocrysts are always adjacent to Fe-rich richterite and/or Na-hedenbergite ones. Phenocrysts in peralkaline trachytes have high Mn (up to 4.2 wt% MnO) and Ti (up to 6.9 wt% TiO_2) contents. Higher contents (6.9 and 8.8 wt% respectively) are found in microlites of phonolites. In peralkaline trachytes and in phonolite R4, aenigmatite is rich in niobium ($0.13 < \text{Nb}_2\text{O}_5$ wt% < 0.45), although not as rich as that from one phonolite of Rumpi Hills, SW Cameroon (Nb_2O_5 wt% ≈ 0.70 ; Farges et al. 1994). Fe contents (0.5 to 1.3 a.p.f.u.) allow calculation of large amounts of Fe-aenigmatite (up to 34%) and of Fe^{3+} -Tschermak (up to 19%) in their respective sites. Contents in CaO (0.1 to 0.5 wt%) and Al_2O_3 (0.5 to 1.7 wt%) are low. Such high Fe^{3+} contents indicate oxygen fugacities lower than those of the FMQ buffer (estimates after Ernst 1962), and such low Ca and Al contents indicate low temperature (estimates after Larsen 1977) during crystallisation. There is no Fe–Ti oxide coexisting with aenigmatite in phonolites and peralkaline trachytes, in conformity with the "no-oxide" field established by Marsh (1975) in a $f\text{O}_2$ T diagram for similar lavas which also contain the Na-pyroxene-aenigmatite association.

Ti-magnetite

In basalts, Ti-magnetite occurs as subhedral crystals enclosed in olivine or Ti-diopside phenocrysts (Fe recalculated after Stormer 1983). In phonolites, Ti-magnetite is Mn-rich and Ti-depleted (12.2–15.9 wt% TiO_2 ; eTable 6). Contents in MnO increase (0.5 to 5.9 wt%) and contents in MgO (4.4 to 0.1 wt%) and Al_2O_3 (6.2 to 0.1 wt%) decrease from basalts to phonolites and trachytes.

Feldspars

The basalts contain plagioclase microlites and microphenocrysts the compositions of which range from $\text{An}_{64}\text{Ab}_{35}\text{Or}_1$ to $\text{An}_{45}\text{Ab}_{51}\text{Or}_4$ (Fig. 8; eTable 7). Hawaiiite K98 contains plagioclase microphenocrysts and microlites of significantly distinct compositions ($\text{An}_{57}\text{Ab}_{41}\text{Or}_2$ and $\text{An}_{28}\text{Ab}_{66}\text{Or}_6$ respectively). The phonolites contain microlites of albite ($\text{An}_2\text{Ab}_{97}\text{Or}_1$) and sanidine ($\text{An}_1\text{Ab}_8\text{Or}_{91}$) and resorbed phenocrysts of albite ($\text{An}_4\text{Ab}_{94}\text{Or}_2$) which are crenellated due to a late overgrowth of sanidine, as in sample R4. The peralkaline trachytes contain phenocrysts of albite

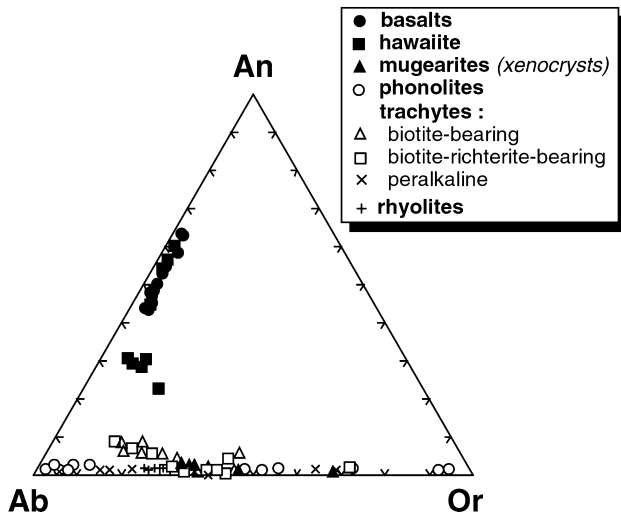


Fig. 8 Compositions of feldspars (mol%) from the Upper Benue valley lavas (microlites in basalts, microlites and microphenocrysts in hawaiites, xenocrysts in mugearites, and phenocrysts in phonolites, trachytes and rhyolites)

(Ab₉₈ to Ab₆₆) and microlites of anorthoclase (Ab₆₉Or₂₉ to Ab₇₃Or₂₅) whereas the other trachytes contain phenocrysts and microlites of anorthoclase (An₅₋₆Ab₅₈₋₅₀Or₂₇₋₄₄). The rhyolites contain alkali feldspar phenocrysts (Or₂₅ to Or₂₉). The evolution of feldspar compositions from albite to sanidine in phonolites and peralkaline trachytes can tentatively be explained by the presence of F-rich fluids which induced decreasing of liquidus temperature and depolymerisation of silicate liquids (Mysen 1991).

Feldspathoids

Nepheline composition (mol%) varies between Ne₈₈Ks₁₂Qz₀ and Ne₅₇Ks₈Qz₃₅ (Fig. 9; eTable 8). Na₂O content varies between 14.8 and 17.2 wt%, and K₂O and recalculated Fe₂O₃ contents are high (up to 4.9 and 1.8 wt% respectively). The temperature of crystallisation of nepheline in phonolite R4 is mostly lower than 700 °C whereas it is higher in phonolite N6 (estimates after Hamilton 1961). Petrographic observations indicate that the nepheline crystallised as a primary phase. In phonolites, analcite and sodalite occur as accessory mineral phases and sodalite is anomalously rich

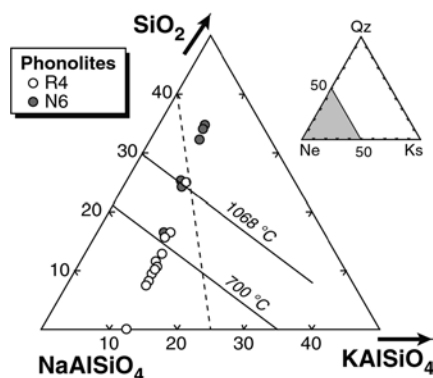


Fig. 9 Compositions of nepheline (mol%) from the Upper Benue valley phonolites. Isotherms (after Hamilton 1961) and the trend (dashed line) of natural low-T nephelines (after Barth 1963) are indicated

in Na₂O and Cl (22.3 and 6.8 wt% respectively). The sodalite + nepheline + sanidine association indicates low pressures of crystallisation (1.6 < P kbar < 2.8; estimates after Wellman 1970).

Xenocrysts

Olivine xenocrysts are easily distinguished from phenocrysts by their rounded shape and their numerous cracks. They occur in basalt 4P together with Cr-spinel xenocrysts. Olivine xenocrysts have higher Mg# (F_{0.92-87}) and Ni contents, and lower Mn and Ca contents than phenocrysts (eTable 1). Their crystallisation temperature (1,265 ± 70 °C, estimate as for phenocrysts, see above) and pressure (7 kbar, estimate after Presnall et al. 1978) correspond to those occurring at the discontinuity between the lower crust and the upper mantle (≈20 km).

Quartz xenocrysts surrounded by a clinopyroxene corona occur in basalt 4P. This pyroxene is Ca-rich (Wo₄₈₋₄₆En₃₈₋₃₇Fs₁₄₋₁₇), poorer in Al (Al₂O₃ < 0.35 wt%) and Ti (TiO₂ < 0.70 wt%) and richer in Na (Na₂O up to 1.45 wt%), Si and Ca than the Ca-rich pyroxene phenocrysts (Fig. 5, eTable 2). Pyroxenes of such composition are commonly observed surrounding quartz xenocrysts in basaltic lavas. High Si and Ca, and low Fe, Ti, and Al contents are generally explained through a reaction between SiO₂ and the basaltic magma. This reaction, which took place at the interface between quartz crystals and the magmatic liquid, illustrates increasing localised silica activity around the quartz crystals.

Mg-rich pyroxene xenocrysts (Di₇₉Hd₁₈Ac₅) occur in phonolite R4. Their composition (Fig. 5) is similar to that of Ca-rich pyroxene phenocrysts found in basalt 4P.

Biotite in mugearites is strongly zoned with a greenish brown core surrounded by a light brown, intermediate zone and a greenish yellow rim, and has a reverse chemical zonation, similar to that sometimes observed in biotite-bearing trachytes (Fig. 7).

Other xenocrysts are sanidine (An₄₋₁Ab₆₅₋₃₂Or₃₁₋₆₇) and apatite in mugearites.

Conclusions

Mineral inspection pinpoints several features:

- the series is of definite alkaline character;
- the presence of olivine, pyroxene and quartz xenocrysts in basalts testifies of wall-rock magma interaction in the crust;
- the occurrence of pyroxene xenocrysts in phonolites with a composition similar to those of the pyroxene phenocrysts of the basalts is a strong argument in favour of magma mixing. The same argument applies for the sanidine and biotite xenocrysts of the mugearite which are similar in composition to the phenocrysts observed in the trachytes;
- the high contents of fluorine (4.6 wt% in arfvedsonite, 2.4 wt% in biotite), chlorine (6.8 wt% in sodalite) and CO₂ (attested by the occurrence of carbonates in all the felsic lavas), and the late transformation of nepheline into analcite stress the important role played by fluids during the crystallisation of mineral phases.

Geochemistry

Overview

Major- and trace-element compositions of selected representative samples of the Upper Benue valley lava series are presented in Table 3. Alkali basalts, hawaiites, mugearites, phonolites, trachytes and rhyolites have been analysed; they all belong to the alkaline series. The

Table 3 Chemical compositions of representative Upper Bueuevalley lavas

Rock type	Basalt				Hawaiite				Phonolite				Biotite-bearing trachyte				Biotite-richterite-bearing trachyte				Peralkaline trachyte				Rhyolite		Gneiss	
	4P	G23	G22	T1	K98	BG3	R4	B2	N6	G5	B8	F9	R112	4G	MD4	R6	4L	F5	4E	MD5	KA4	MU1	F3	IN4	IN4	IN4		
(wt%)	43.01	43.28	42.53	41.75	43.56	53.57	59.28	60.19	60.34	60.95	62.02	64.74	66.74	66.07	64.87	64.40	65.62	65.29	67.47	67.10	63.80	64.02	72.32	76.31				
SiO ₂	2.87	2.95	3.65	3.65	3.34	1.29	0.20	0.12	0.15	0.25	0.44	0.69	0.68	0.22	0.27	0.25	0.43	0.15	0.31	0.22	0.24	0.14	0.12	<0.05				
TiO ₂	12.96	12.96	13.73	13.66	16.78	16.58	19.71	19.22	19.39	18.82	17.32	16.35	15.60	16.82	16.14	17.23	17.20	16.68	17.71	17.01	16.03	16.60	13.53	13.17				
Fe ₂ O ₃ *	13.30	13.21	15.86	15.91	11.39	6.56	3.06	2.84	3.00	3.08	4.92	3.79	3.08	3.46	4.44	3.77	3.87	3.54	2.08	1.77	4.49	3.95	2.09	0.76				
MnO	0.18	0.17	0.26	0.27	0.25	0.30	0.26	0.26	0.25	0.27	0.22	0.04	0.20	0.50	0.30	0.08	0.32	0.02	0.00	0.42	0.44	0.15	0.15	<0.03				
MgO	9.54	10.03	5.82	5.89	3.79	1.00	0.05	0.03	0.03	0.10	0.16	0.30	0.22	0.14	0.26	0.14	0.00	0.11	0.00	0.22	0.22	0.10	0.08	<0.01				
CaO	9.41	9.33	9.14	9.53	9.75	6.19	1.04	0.92	1.01	0.91	0.80	0.51	0.98	0.13	0.36	0.56	0.37	0.44	0.10	0.45	0.52	0.68	0.32	0.60				
Na ₂ O	4.03	4.00	4.25	4.29	4.24	5.51	9.42	9.07	8.46	8.66	5.69	5.49	5.27	5.30	6.09	6.37	5.97	6.68	5.33	6.26	7.44	7.51	5.75	2.81				
K ₂ O	1.24	1.38	2.04	1.82	2.27	2.83	4.97	5.15	5.20	5.41	5.50	6.00	5.57	5.20	5.17	5.27	5.37	5.32	5.65	5.44	5.10	5.16	4.41	5.19				
P ₂ O ₅	0.76	0.81	1.52	1.56	1.16	0.53	0.08	0.09	0.07	0.05	0.16	0.20	0.52	0.00	0.13	0.08	0.05	0.06	0.00	0.08	0.25	0.00	0.05	<0.05				
L.O.I.	98.96	99.56	99.53	99.77	99.06	99.51	99.63	99.68	99.72	99.69	99.60	99.58	99.77	99.97	99.49	99.37	100.32	99.47	100.42	100.13	99.14	99.24	99.66	99.69				
Total	31.88	32.07	37.65	36.03	40.32	65.16	87.87	88.30	89.36	94.61	82.55	87.62	88.79	86.76	86.92	87.59	99.28	90.02	90.61	94.36	85.00	87.10	92.23	92.67				
D.I.																												
(ppm)	2.1	2.2	2.5	2.7	2.2	2.9	5.1	8.8	4.0	5.3	1.3	2.0	0.8	5.0	3.5	5.0	7.8	7.8	2.7	6.7	9.9	14.6	2.3					
Be	33	39	29	45	58	38	219	227	190	221	141	128	144	150	182	159	202	339	203	168	246	453	164					
Rb	963	969	1,390	1,483	1,650	1,303	145	10	18	65	87	33	67	52	53	122	68	23	35	24	19	29	112					
Sr	711	672	699	712	988	1,016	189	11	55	163	1,258	265	1,538	397	141	961	591	126	205	120	170	78	35	495				
Ba	223	222	213	215	197	19	<5	<5	6	<5	<5	6	11	33	<5	<5	<5	<5	<5	<5	<5	<5	<5	<5				
V	27	53	55	47	21	9	7	<5	7	8	<5	6	6	<5	9	<5	<5	<5	<5	<5	<5	<5	<5	<5				
Cu	225	251	10	11	6	9	<5	<5	<5	<5	<5	<5	<5	<5	<5	<5	<5	<5	<5	<5	<5	<5	<5	<5				
Cr	50	44	27	29	14	<5	<5	<5	<5	<5	<5	<5	<5	<5	<5	<5	<5	<5	<5	<5	<5	<5	<5	<5				
Co	209	232	33	33	12	<5	8	<5	<5	<5	<5	<5	<5	<5	<5	<5	<5	<5	<5	<5	<5	<5	<5	<5				
Ni	23	22	17	17	11	7	1	1	1	1	1	3	3	3	1	3	1	1	1	1	2	2	1	<1				
Sc	121	122	149	146	124	128	160	187	144	128	76	101	82	177	122	177	141	141	62	186	233	237	15					
Zn	121	124	138	135	131	27	33	30	31	113	28	16	16	25	33	25	33	17	32	10	27	25	17					
Ga	31	28	38	41	38	45	36	41	31	47	23	34	29	50	49	34	34	38	48	50	69	47	12					
Y	315	313	494	500	408	494	1,186	1,000	1,022	1,121	631	568	391	780	773	780	882	882	754	880	1,000	729	63					
Zr	109	107	157	141	138	95	184	196	171	235	100	99	78	211	152	211	167	167	157	262	313	431	4					
Nb	77.9	67.8	104.0	113.0	93.2	84.6	135.0	140.9	169.9	140.9	99.6	79.5	177.4	100.1	125.9	100.1	100.1	138.6	194.5	177.4	73.0	73.0	17.9					
La	139	120	193	207	174	174	201	207	207	249	185	143	237	158	206	158	206	207	218	237	104	30	30					
Ce	57.1	52.9	91.2	99.3	80.9	82.2	45.7	13.8	67.2	72.7	59.6	96.8	72.7	57.0	65.6	57.0	65.6	80.7	107.9	96.8	28.3	28.3	17.1					
Nd	11.4	11.1	16.7	17.5	15.3	16.1	7.3	6.5	11.0	12.6	10.1	15.5	12.6	10.0	10.8	10.0	10.8	13.8	17.6	15.5	5.7	5.7	4.2					
Sm	3.28	3.31	4.85	5.24	4.53	4.65	1.14	1.01	1.85	2.46	2.82	1.74	2.46	1.73	0.90	1.73	0.90	1.38	1.71	1.74	0.66	0.66	0.76					
Eu	8.9	9.1	12.9	14.1	12.1	13.0	6.5	5.6	9.2	9.3	7.4	10.5	9.3	7.0	8.2	7.0	8.2	9.6	12.1	10.5	5.0	5.0	3.6					
Gd	6.2	5.9	8.3	9.0	8.1	9.0	5.3	4.7	7.2	6.7	5.5	7.8	6.7	5.6	6.7	5.6	6.7	7.8	9.2	7.8	5.7	5.7	2.5					
Dy	2.4	2.4	3.2	3.3	3.2	5.0	3.5	3.1	4.2	3.4	2.6	4.1	3.4	3.0	3.7	3.0	3.7	4.1	4.8	4.1	4.0	4.0	1.1					
Er	1.76	1.73	2.69	2.84	2.68	3.36	3.99	3.51	4.88	2.85	2.16	4.33	2.85	3.20	3.62	3.20	3.62	4.43	4.16	4.33	4.85	4.85	1.08					
Yb	0.24	0.26	0.36	0.38	0.34	0.60	0.72	0.62	0.70	0.51	0.35	0.67	0.51	0.52	0.63	0.52	0.63	0.69	0.71	0.67	0.81	0.81	0.15					
Lu	8.0	8.0	11.0	12.0	12.0	10.0	33.0	34.0	31.0	24.0	15.0	14.0	14.0	10.0	26.0	10.0	25.0	27.0	27.0	22.0	36.0	51.0	16.2					
Th																												

^aDetails about the analytical procedures (ICP and ICPMS, CNRS, CRPG, Nancy) can be found in Carignan et al. (2001). Differentiation index (D.I., Thornton and Tuttle 1960) is deduced from the CIPW norms which were calculated assuming a FeO/Fe₂O₃ ratio of 0.15 for the basaltic lavas, and 0.3 for the felsic ones. Data for IN4 gneiss sample from the Pan-African basement have also been indicated

basaltic lavas (alkali basalts and hawaiites), the mugearites, the phonolites and the peralkaline trachytes contain normative nepheline (12.5 to 14.0%, 1.0 to 2.3%, 13.5 to 20.6%, and 0.5 to 1.8% respectively). Other trachytes and rhyolites are quartz normative (2.3 to 13.7% and 18.8 to 20.9% respectively). Basaltic lavas have moderate MgO contents (5.8 to 10.0 wt%). Mugearites ($61.6 < D.I. < 65.2$) plot between basaltic ($D.I. < 40.3$) and felsic lavas ($D.I. > 82.5$) in all element–element diagrams. These intermediate lavas disrupt the clear bimodality of the series, contrarily to what has been observed on the Kapsiki plateau, 200 km northwards (Ngounouno et al. 2000). In biotite-bearing and biotite-richterite-bearing trachytes, normative corundum is present. This is not an artefact resulting from weathering because these lavas are petrographically fresh (as attested by microscope observation) and have rather low LOI contents, as all other lavas (except

mugearites), and also because they are peraluminous (molecular $(Na + K + Ca)/Al < 1.0$).

Major and trace elements

Major- and trace-element distributions vs. Rb content are presented in Figs. 10 and 11. Rubidium has been used as a differentiation index because of its large range of variation (from 30 ppm in basalts to 230 in phonolites and to 450 ppm in rhyolites), and because this element is strongly incompatible and is excluded from the fractionation processes.

Silica content increases with differentiation except in phonolites where it is less abundant than in trachytes. TiO_2 , $Fe_2O_3^*$ and CaO contents are high in basaltic lavas (3.6, 16.0, and 9.8 wt% respectively) and decrease strongly in felsic lavas. MgO and P_2O_5 also decrease

Fig. 10 Major-element variation diagrams vs. Rb for Upper Benue valley lavas (see text for explanation)

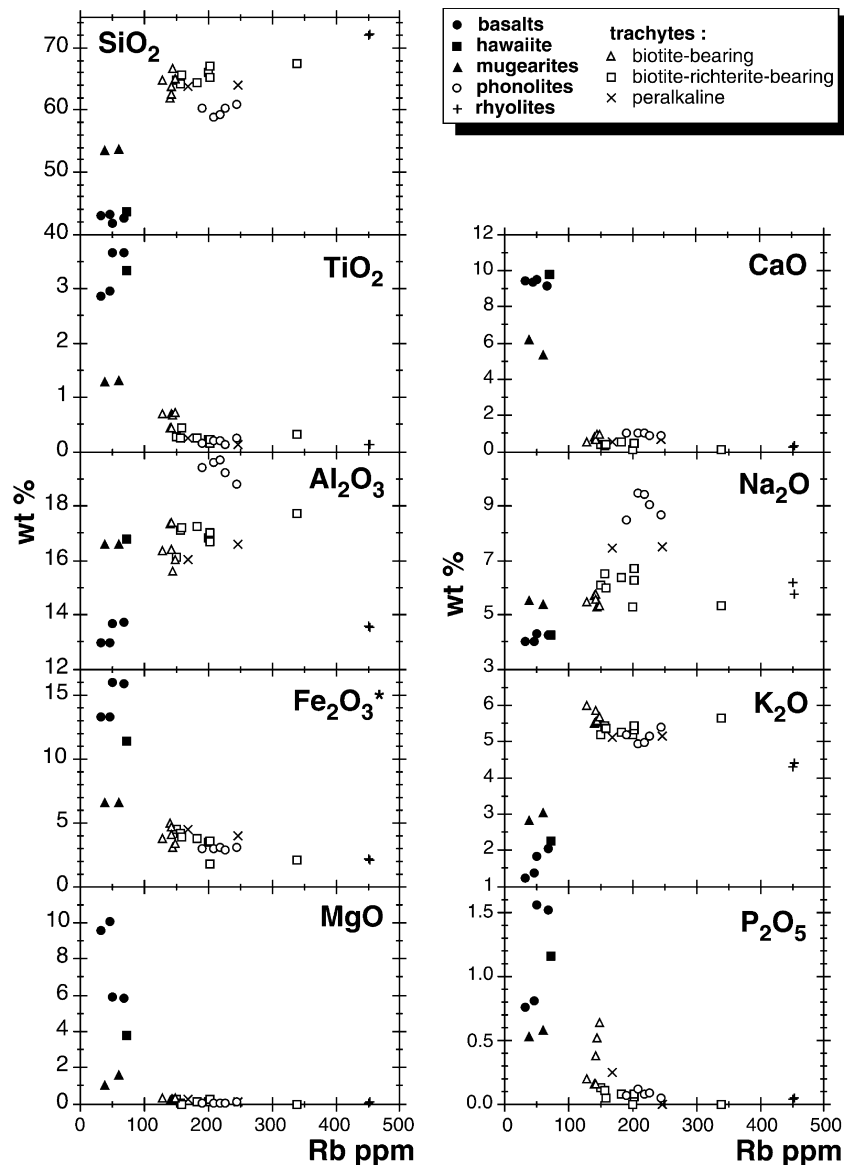
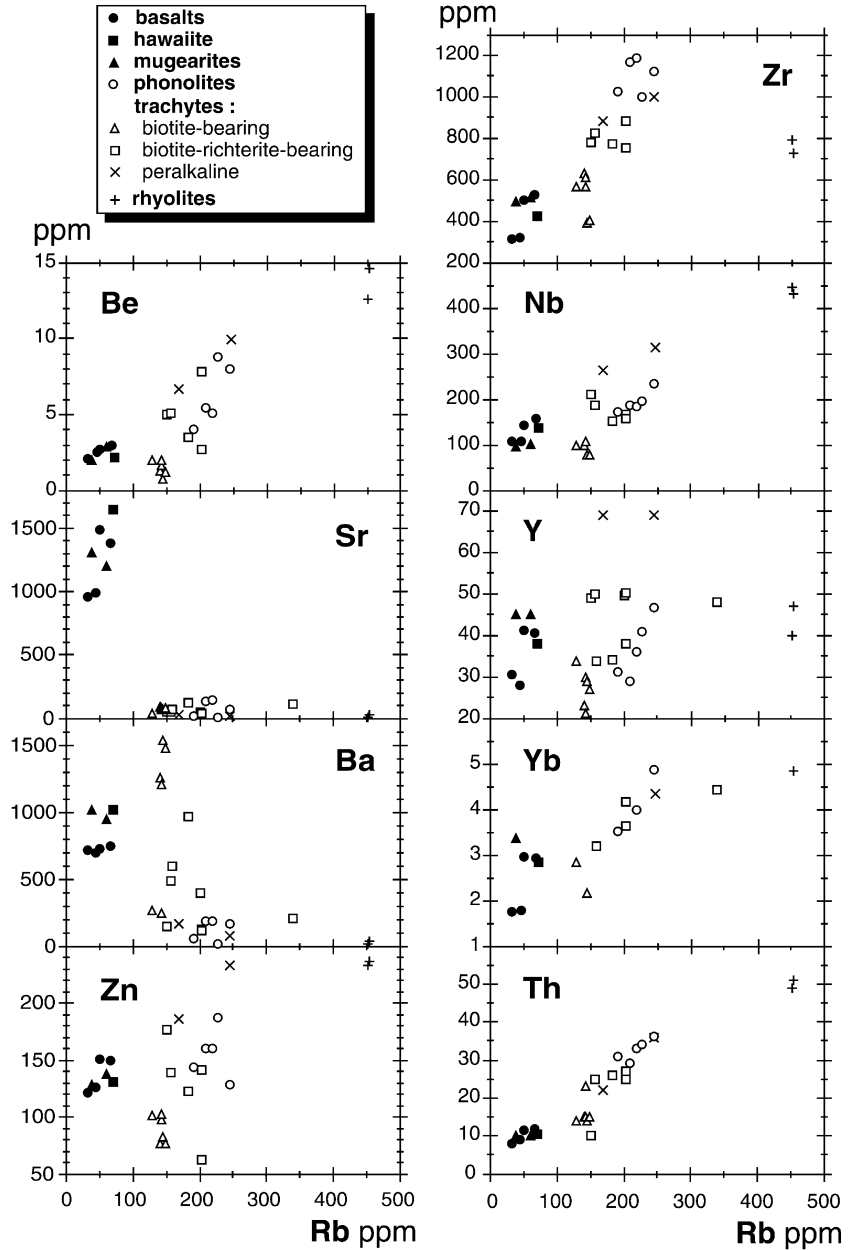


Fig. 11 Trace-element distributions vs. Rb for Upper Benue valley lavas



drastically: the MgO content is typically less than 0.30 wt%, and the P₂O₅ content less than 0.25 wt% in felsic lavas (except in biotite-bearing trachytes). The aluminium content is low in basalts and rhyolites (Al₂O₃ wt% < 13.8) and is higher in phonolites (18.8 < Al₂O₃ wt% < 19.7). Compared to basalts, hawaiiite and mugearites have high aluminium content (Al₂O₃ wt% ≈ 16.6). The Na₂O contents and Rb concentrations (≈ 40 ppm) in basalts are similar to those for other basalts from the Cameroon Line (e.g. Mt Cameroon, Déruelle et al. 2000) with similar D.I. (≈ 30). Mugearites, biotite-bearing trachytes, and rhyolites have similar Na₂O content (≈ 5.5 wt%) but peralkaline trachytes, and above all phonolites have much higher content (Na₂O wt% up to 9.4 in phonolites). The content in K₂O increases from basalts and hawaiiite

(1.2 < K₂O wt% < 2.3) to biotite-bearing trachytes (up to 6.0 wt%); then it regularly decreases with differentiation (K₂O wt% ≈ 4.4 in rhyolites).

Only two basalts have high transition metal element contents (Ni and Cr ppm > 200, Co ppm > 40, and Sc ppm > 20); the other basalts have very low contents of these elements. In felsic lavas the abundances of metal transition elements (V, Cu, Cr, Co, and Ni) are usually below the analytical detection limit. Zinc is high (> 200 ppm) in rhyolites and one peralkaline trachyte. Beryllium contents increase from basalts (23 ppm) to rhyolites (up to 15 ppm), except for biotite-bearing trachytes which have low Be contents (≈ 2 ppm) near the analytical detection limit (0.9 ppm).

Basalts, hawaiiites and mugearites are characterised by high Sr and Ba contents (Sr > 960 ppm and

Ba > 670 ppm) and Sr/Ba ratios comprised between 1.3 and 2.0, but Sr contents are low (< 150 ppm) in felsic lavas. Biotite-bearing trachytes reveal high Ba contents (> 1,200 ppm) and moderate to low Sr contents (87–67 ppm); accordingly, Sr/Ba are about 0.1. Other types of trachytes yield low Sr/Ba ratios varying between 0.1 and 0.5, reflecting high to moderate Ba contents and moderate to low Sr contents. Contents in zirconium increase from basaltic lavas and mugearites (250 to 500 ppm) to biotite-bearing trachytes (400 to 600 ppm) and phonolites (~1,200 ppm) but decrease in rhyolites (800 ppm). Contents in niobium are low in biotite-bearing trachytes (80 to 110 ppm), basaltic lavas, and mugearites (95 to 155 ppm), but higher in biotite-richterite-bearing trachytes, phonolites and peralkaline trachytes (up to 315 ppm), and even higher in rhyolites (~450 ppm). The Zr/Nb ratios are nearly constant (around 4) for the whole series, from basalts to phonolites and peralkaline trachytes (Fig. 12). The rhyolites have drastically lower Zr/Nb ratios (~1.7), possibly due to aegirine-augite (up to 1.07 wt% ZrO₂) and aenigmatite (up to 0.16 wt% ZrO₂) fractionation in the peralkaline trachyte magma. Yttrium contents range between 20 and 50 ppm for all the lavas (biotite-bearing trachytes having the lowest Y contents), except for the peralkaline trachytes (~70 ppm). Concentrations in Yb are higher in felsic lavas than in basaltic ones, except in biotite-bearing lavas. Thorium contents increase regularly from basalts to rhyolites, but biotite-bearing trachytes and biotite-richterite-bearing trachyte MD4 plot below the main trend.

All the Upper Benue valley basalts are rich in light-REEs (Fig. 13a) and have high (Ce/Yb)_N (16.8–20.4) compared to those of basalts with similar D.I. values (30 < D.I. < 38) from the Kapsiki plateau (Ngounouno et al. 2000) and Mt Cameroon (Déruelle et al. 2000). The REE distributions of the basalts and hawaiiite are

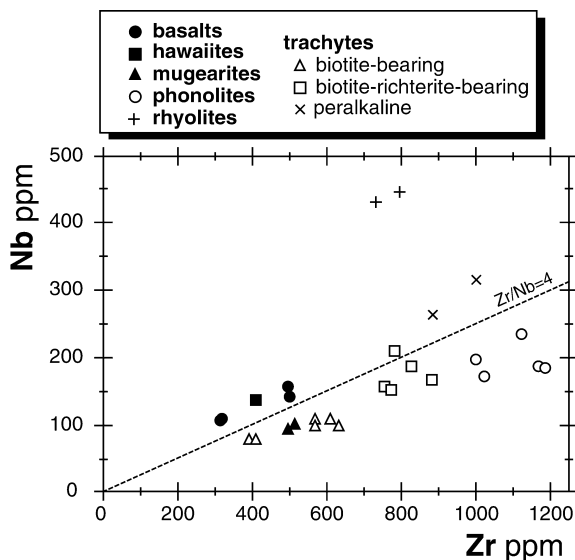


Fig. 12 Zr–Nb diagram for Upper Benue valley lavas

quite similar, with high (La/Yb)_N ratios (23.5–29.9) and (La/Sm)_N ratios varying between 3.8 and 4.3. Normalised patterns show a regular decrease from La to Lu, with a steep slope and no europium anomaly. By contrast, felsic lavas display various distributions (Fig. 13b):

- biotite-bearing trachytes yield normalised patterns close to those of basalts, with (La/Yb)_N ratios ≈ 24 and (La/Sm)_N ratios ≈ 5;
- phonolites show (La/Yb)_N ratios comprised between 22.8 and 27.1, high (La/Sm)_N ratios between 9.7 and 13.6, and pronounced negative europium anomalies (Eu/Eu* = 0.5);

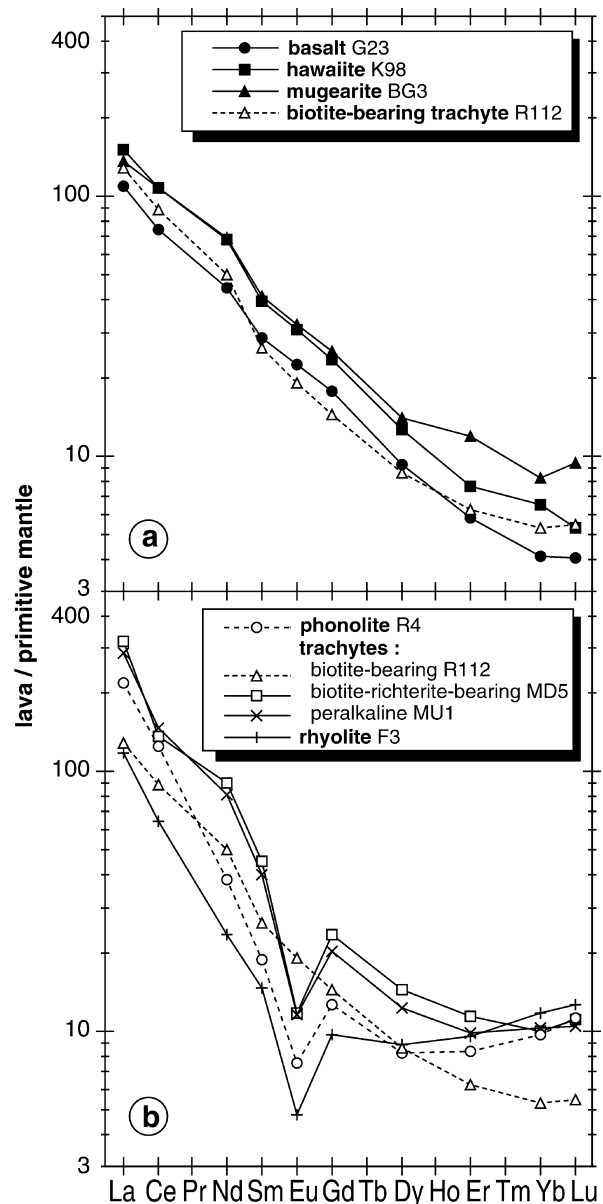


Fig. 13a, b Primitive mantle-normalised REE diagrams for a basalt, hawaiiite, mugearite and biotite-bearing trachyte; and b phonolite, trachytes and rhyolite from the Upper Benue valley (normalisation data after Hofmann 1988)

- biotite-richterite-bearing and peralkaline trachytes have somewhat different $(La/Yb)_N$ ratios (21.1–31.6) whereas they all display remarkably constant $(La/Sm)_N$ ratios (6.3–7.3) and significant negative Eu anomalies;
- mugearite yields a peculiar REE pattern relative to other felsic rocks, with low $(La/Yb)_N$ and $(La/Sm)_N$ ratios (17.0 and 3.3 respectively) and no Eu anomaly;
- rhyolite is also remarkable in the REE distribution, with a low $(La/Yb)_N$ ratio (10.2), high $(La/Sm)_N$ ratio (8.1), quite high HREE contents, and a well-defined negative Eu anomaly.

Sr and Nd isotopes

Samples for Rb–Sr and Sm–Nd isotopic analyses were dissolved in mixed HF–HNO₃ (10:1), and chemical separation was carried out by cation-exchange chromatography; blanks were < 1 ng. Sr and Nd isotopic ratios were measured on a VG Sector 54 multicollector thermal ionisation mass spectrometer. Replicate analyses of the Merck Nd standard gave an average ¹⁴³Nd/¹⁴⁴Nd value of 0.512742 ± 8 (normalised to ¹⁴⁶Nd/¹⁴⁴Nd = 0.7219), and measurements of NBS 987 Sr yielded an average ⁸⁷Sr/⁸⁶Sr value of 0.710247 ± 7 (normalised to ⁸⁶Sr/⁸⁸Sr = 0.1194). Epsilon Nd values were calculated assuming ¹⁴⁷Sm/¹⁴⁴Nd = 0.1967 and ¹⁴³Nd/¹⁴⁴Nd = 0.512638 for CHUR (after Ashwal et al. 2002).

Sr isotopic composition has been measured for the whole sequence of lavas (basalts, hawaiite, mugearite, phonolites, various trachytes, and rhyolites, Table 4). Initial isotopic compositions (Sr_i) have been recalculated at 37 Ma. The basalts have uniformly low Sr_i values of 0.70340 ± 0.00003 . The phonolites (0.7034–0.7042) and mugearite (0.7048) are slightly higher. The trachytes are quite variable—their Sr_i range from 0.7065 to 0.7106 (for KA4 peralkaline trachyte). The rhyolite also has a high Sr_i of 0.7107.

Some Nd isotopic measurements have been performed (Table 4). The four analysed samples have positive $\epsilon Nd_{(37\text{ Ma})}$ values, ranging from + 3.9 for the basalt and phonolite down to + 0.4 for the rhyolite. The $\epsilon Nd_{(37\text{ Ma})}$ value for the single analysed trachyte is + 3.9.

Sr and Nd isotopic compositions for a gneiss sample (IN4, Table 4) from the neighbouring Pan-African basement (⁸⁷Sr/⁸⁶Sr_(37 Ma): 0.74900; $\epsilon Nd_{(37\text{ Ma})}$: –11.9) are typical of the continental crust.

Discussion

Basalts contain phenocrysts of olivine (F_{085–68}), Al-Ti-rich diopside and Ti-magnetite and xenocrysts of olivine (F_{092–87}) with Cr-Ti-rich spinel inclusions, and of quartz. The hawaiites contain abundant plagioclase microphenocrysts and Al-Ti-diopside phenocrysts. The

Table 4 Strontium and neodymium isotopic compositions. Rb and Sr have been measured by high-precision XRF unless otherwise indicated (see tablenotes). Data for the IN4 gneiss sample from the Pan-African basement have also been indicated

Rock type	Sample			Strontium				Neodymium					
	Rb (ppm)	Sr (ppm)	(ppm)	⁸⁷ Rb/ ⁸⁶ Sr	⁸⁷ Sr/ ⁸⁶ Sr	2σ	(⁸⁷ Sr/ ⁸⁶ Sr) _{37 Ma}	Sm (ppm)	Nd (ppm)	¹⁴⁷ Sm/ ¹⁴⁴ Nd	¹⁴³ Nd/ ¹⁴⁴ Nd	2σ	$\epsilon Nd_{37\text{ Ma}}$
Basalt	4P	37.7	957		0.703480	0.000011	0.70342						
	G23	38.2	953	0.114	0.703436	0.000010	0.70338	17.5	99.3	0.1066	0.512814	0.000011	+ 3.86
	T1	41	1,426	0.083	0.703407	0.000011	0.70336						
Mugearite	BG1	61	1,176	0.151	0.704904	0.000008	0.70483	7.3	45.7	0.0987	0.512814	0.000010	+ 2.06
	R4	211	139	4.393	0.705946	0.000008	0.70364						
Phonolite	G5	210	61.8	9.838	0.709364	0.000010	0.70419						
	R111	140	71.5	5.669	0.711197	0.000010	0.70822						
Biotite-bearing trachyte	4L	154	55.7	8.006	0.710781	0.000010	0.70657	17.6	107.9	0.0966	0.512720	0.000008	+ 3.91
	MD5	203 ^b	35 ^b	16.805	0.717407	0.000009	0.70858						
Peralkalinetrachyte	KA4	151	23.5 ^a	18.593	0.720436	0.000011	0.71065	5.7	28.3	0.1218	0.512639	0.000010	+ 0.37
	F3	453 ^b	29 ^b	45.335	0.734494	0.000007	0.71067	4.2	17.1	0.1495	0.512015	0.000009	–11.92
Rhyolite	IN4	164	112	4.257	0.751236	0.000012	0.74900						

^aSample measured by isotope dilution mass spectrometry

^bSamples measured by ICPMS (see Table 3)

mugarites have a trachytic texture and contain magnetite phenocrysts, xenocrysts of sanidine, quartz, and biotite. Phonolites are peralkaline with Na-hedenbergite, \pm Mg-hastingsite, aegirine-augite, Ti-aenigmatite, nepheline and albite phenocrysts; they also contain microphenocrysts of sodalite, sphene, apatite, and xenocrysts of Ca-rich diopside. Two types of trachytes occur. Peralkaline trachytes contain phenocrysts of aegirine-augite, richterite, arfvedsonite, aenigmatite, albite and sanidine-anorthoclase. Non-peralkaline trachytes are classified into two groups: biotite-bearing trachytes with phenocrysts of Ba-Ti-rich biotite and Ti-magnetite and biotite-richterite-bearing trachytes. The rhyolites are peralkaline, with Ti-aegirine-augite and F-Mn-arfvedsonite microphenocrysts.

The Upper Benue valley lavas and the "Daly gap"

In major-element distribution diagrams for co-magmatic alkaline lavas series, a compositional gap is systematically observed between basaltic lavas and felsic ones, the lack of lavas of intermediate composition ("Daly gap") being a characteristic feature of many alkaline series. This is also the case for the Upper Benue valley lava series: excepting the mugarite with SiO_2 wt% = 53.6 (the petrogenesis of which will be discussed below), there is no lava in the silica range 48–59 wt% SiO_2 . The gap is also clearly observed in TiO_2 , CaO, Fe_2O_3^* , K_2O distributions (Fig. 10). Sampling cannot be invoked for this peculiar distribution because all lava outcrops have been systematically sampled as the result of a painstaking fieldwork. Three hypotheses have been put forward recently to explain such a compositional gap: (1) the gap may be a consequence of the failure of intermediate magmas to erupt because of a rapid differentiation over a narrow temperature range (MacDonald 1987), (2) the gap may result from small variations in magma residence time, and cooling rate which may induce a magmatic bifurcation interrupting the liquid line of descent (Bonnefoi et al. 1995), and (3) the gap may result from crystal fractionation which increases the viscosity and inhibits eruption of magmas with intermediate composition (Thompson et al. 2001).

As already stated for the Cameroon Line (see Ngounouno et al. 2000), it is a long-standing question whether the quartz-normative trachytes (on a CIPW-normative basis) and the alkaline rhyolites which commonly occur in continental settings conjointly with basaltic lavas represent extreme differentiates of the associated basalts or are derived from some other processes. In the first hypothesis, the suites are qualified as bimodal (co-magmatic) and genetically related by fractional crystallisation (Nigerian Upper Benue: Grant et al. 1972; Adamawa: Nono et al. 1994) whereas in the second one, both basaltic and felsic lava groups are considered to be independent and thus have distinct genesis, the former being related to mantle-derived magmas and the latter to crustal anatexis (Deccan Trap:

Lightfoot et al. 1987; Basin and Range Province: Draper 1991).

In the following discussion, it will be shown that the basalts and rhyolites of the Upper Benue valley are not simply related by a fractional crystallisation process from mantle-derived magmas, but that crustal contamination, magma mixing, and fluids have played a significant role in the genesis of the felsic lavas.

Origin of the basaltic lavas

Among the Upper Benue valley basalts, only two (4P, G23) have high MgO contents (≈ 10.0 wt%; $\text{Mg}\#\approx 60$) and high Ni and Cr contents (> 200 ppm). Although the mantle origin of the magmas from which these basalts originated is certain (occurrence of Fo_{92-87} olivine and Cr-spinel xenocrysts), these basalts are not primitive. They are similar to those with identical or lower D.I. values from volcanoes from the Cameroon Line (Mt Cameroon: Déruelle et al. 2000; Kapsiki plateau: Ngounouno et al. 2000) and Adamawa (Tchabal Nganha: Nono et al. 1994). The other two basalts (G22, T1) and the hawaiiite (K98) of the Upper Benue valley contain significantly less magnesium (MgO wt% < 5.9 ; $\text{Mg}\#\approx 42$), nickel ($\text{Ni} < 33$ ppm) and chromium ($\text{Cr} < 11$ ppm). This is strong evidence of olivine \pm clinopyroxene \pm Fe-Ti-oxide fractionation in the genesis of the Upper Benue valley basalts. Modelling of the major-element distribution by mass-balance crystal fractionation has been attempted, using the compositions of the fractionated mineral phases (olivine, clinopyroxene and Ti-magnetite from eTables 1, 2 and 6 respectively). The occurrence of quartz xenocrysts in the presumed basalt parents (4P and G23) has also been taken into account by subtracting 0.5 wt% SiO_2 . This modelling gave the sum of squares of residuals lower than 1.8.

The initial isotopic composition of the basaltic lavas ($\text{Sr}_i \approx 0.70340$, $\epsilon \text{Nd} \approx +3.9$) is similar to those of basalts from both the oceanic and continental segments of the Cameroon Line (Halliday et al. 1988; Ngounouno et al. 2000; Demaiffe et al., unpublished data) and Adamawa (Nono et al. 1994; Marzoli et al. 2000). The quartz xenocrysts occurring in some basalts (4P, G23) do not have any detectable influence on the Sr isotopic composition.

The similar trace-element patterns and the comparable isotopic compositions of the Upper Benue valley basaltic lavas and of other basalts from the continental and oceanic sectors of the Cameroon Line (Fitton 1987) and of Adamawa (Nono et al. 1994; Marzoli et al. 2000) are strong arguments in favour of a common mantle source. Pb and Hf isotopic compositions (Halliday et al. 1988; Ballentine et al. 1997) suggest a HIMU-type source. Nevertheless, high $(\text{Ce}/\text{Yb})_N$ values (18–20) for the Upper Benue valley magmas, when compared to those for other basalts of the Cameroon Line (e.g. $(\text{Ce}/\text{Yb})_N \approx 15$ for Mt Cameroon basalts), may reflect very low degrees of partial melting of the mantle source. It

has already been stated that this source is probably located in the asthenosphere or below, since it is obvious that the young (<140 Ma) oceanic lithosphere and the old (>500 Ma) continental lithosphere have followed totally different evolutions since their genesis, and that their present-day geochemical and isotopic signatures are clearly distinct.

Origin of the mugearites

These lavas have a mineralogical composition and a texture similar to those of biotite-bearing trachytes but their chemical composition is more akin to those of basaltic lavas. They contain xenocrysts (≈ 10 vol%) of sieve-textured sanidine, rounded quartz, apatite and biotite (Table 2; Fig. 7). In geochemical diagrams (Figs. 10, 11 and 12), the mugearites plot on the evolution trends of the Upper Benue valley lavas, between the mafic and felsic ones, that is, in the Daly gap. The Sr_i value of BG1 (0.7048) is significantly higher than that of basalts (≈ 0.7034) but its high Sr content ($\approx 1,200$ ppm), similar to those of basalts and hawaiite (950–1,425 ppm), seems to preclude bulk crustal assimilation. The occurrence of quartz and sanidine xenocrysts (1.4 and 4.7 vol% respectively) can account for both the slight increase in SiO_2 (≈ 4.2 wt%) and the higher Sr_i value. Modelling of mass-balance mixing between basalt (or hawaiite) and biotite-bearing trachyte can explain the SiO_2 content of the mugearites but failed to explain the MgO, CaO and K_2O contents. In fact, calculated contents for MgO, CaO and K_2O (2.20, 3.81, and 4.38 wt%) are distinct from the measured values (1.06, 6.56 and 3.00 wt% respectively). This

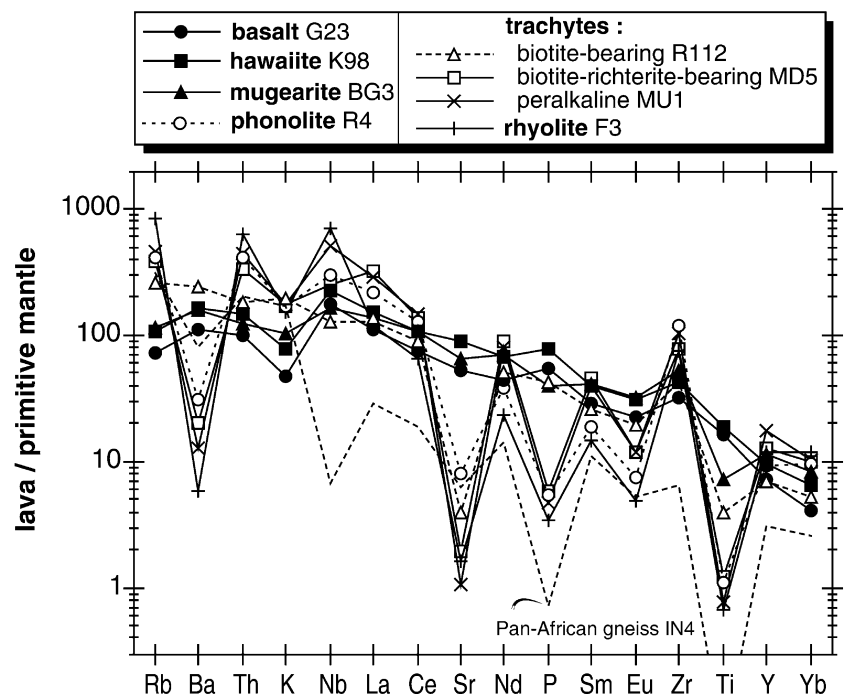
implies that materials other than the Benue lavas should be considered in the modelling. It is suggested that the mugearite results from the mixing, at shallow crustal levels, of a large fraction of a phenocryst-bearing (quartz and sanidine) trachytic magma with a minor amount of basaltic magma. Such mixings between basaltic and felsic magmas are commonly observed in North Cameroon volcanics, i.e. at Tchabal Djinga (Ezangono et al. 1995) and the Kapsiki plateau (Ngounouno et al. 2000), and the resulting mixed lavas have compositions in the range hawaiite–mugearite–benmoreite.

Origin of the phonolites and trachytes

The systematic low contents of TiO_2 , $Fe_2O_3^*$, MgO, CaO, and P_2O_5 (Fig. 10), and of V, Cr, and Ni (Table 3) in Upper Benue valley phonolites and trachytes are qualitatively easily interpreted in terms of fractional crystallisation of Fe–Ti oxides \pm olivine \pm clinopyroxene \pm apatite. The depletion of Ba, Sr and, to a lesser extent, Eu may result from fractionation of feldspar (Fig. 14).

Although two types of phonolite may be distinguished according to the presence or absence of hastingsite, their compositions are similar. Their spoon-shaped REE patterns (Fig. 13) indicate fractionation of amphibole \pm aegirine-augite \pm sphene \pm apatite (Mahood and Stimac 1990). Their normalised trace-element patterns are quite similar to those of the other felsic lavas (except the biotite-bearing trachytes), and therefore significantly distinct from those of basaltic lavas (Fig. 14). However, the initial isotopic compositions of

Fig. 14 Primitive mantle-normalised multi-element diagrams for Upper Benue valley lavas. A Pan-African gneiss (IN4) from the surrounding area is also indicated (normalisation data after Hofmann 1988)



the phonolites ($Sr_i \approx 0.7036-0.7042$; ϵNd values $\approx +2.1$) are only slightly more radiogenic than those of basalts ($Sr_i \approx 0.7034$; ϵNd values $\approx +3.9$), suggesting a mantle source of similar composition. Furthermore, the trace-element patterns of Upper Benue valley phonolites and non-peralkaline phonolites of Tchabal Nganha and the Kapsiki plateau are quite similar, and a mantle source origin has also been proposed for the latter (Nono et al. 1994; Ngounouno et al. 2000). Nevertheless, the relatively low Ba contents (< 190 ppm) of the Upper Benue valley phonolites, compared to Kapsiki phonolites (780 ppm), imply the presence of residual phlogopite in the mantle source region of the former.

Major-element modelling of the basalt-trachyte evolution, through the hawaiite and mugearite compositions, leads to very small proportions of trachytic residual liquid (≈ 0.6 wt%), with $\sum r^2 > 15$. This precludes an evolution through a closed-system fractional crystallisation process alone. Nevertheless, fractional crystallisation modelling has been attempted for evolution from biotite-richterite-bearing trachyte (4L) to peralkaline trachyte (MD5). The least-square mass-balance modelling failed, using the compositions of the mineral phases previously analysed by electron microprobe (K-feldspar, biotite, richterite, arfvedsonite, aenigmatite, and aegirine-augite, eTables 2 to 7), as the sum of the squares of the residuals remained higher than 1.8.

Some biotite-bearing trachytes have high P_2O_5 contents (up to 0.50 wt%), compared to those of other felsic lavas (< 0.25 wt%). They also have high modal apatite content (up to 1.9 vol%; Table 2). So, apatite may have crystallised late in these lavas, and P fractionation could thus be ineffective. Most biotite-bearing trachytes have higher Ba contents (1,200–1,500 ppm) than basaltic lavas (Figs. 11 and 14). So, biotite, which is quite Ba-rich (5.5 to 6.2 wt% BaO), may also have crystallised late in these lavas, and Ba fractionation would thus also be ineffective. These trachytes do not present any negative Eu anomaly (Fig. 13) and thus have not undergone intensive feldspar fractionation. They have relatively low incompatible-element contents compared to other trachytes. Their trace-element-normalised patterns are roughly parallel to those of basalts (except Sr, Ti) and distinct from those of all other felsic lavas in the Upper Benue valley.

On the contrary, fractionation of apatite, biotite, and feldspar has been effective in biotite-richterite-bearing trachytes, as shown by the strong P, Ba, Sr and Eu depletions (Fig. 14). Depletion in light and middle REEs (Fig. 13) may result from apatite fractionation, according to its high partition coefficients for these elements (Mahood and Stimac 1990).

Origin of the rhyolites

Various hypotheses are usually proposed to explain the genesis of alkaline rhyolites in continental settings:

- simultaneous fractional crystallisation of basaltic magmas and their contamination by continental crust (e.g. DePaolo 1981);
- partial melting of the continental crust and melt assimilation by mantle-derived basaltic magmas during their more or less long ascent through the continental crust (e.g. Creaser et al. 1991); and
- partial melting of metasomatised mantle under fluid-rich conditions (e.g. MacDonald 1987).

The relative importance of these processes varies from author to author.

Origin of the Benue rhyolites through a crystal fractionation process using peralkaline trachytes as hypothetical parent magma (with their K-feldspar and aegirine-augite as removed mineral phases) is unrealistic, because of too high SiO_2 and too low Al_2O_3 concentrations in the rhyolite. In trace-element versus Rb abundance diagrams (Fig. 11), the rhyolites plot along the extension of the trends determined by most Upper Benue valley lavas for Nb and Th, and for Sr and Ba which are strongly depleted (≈ 30 ppm). Compared to phonolites and peralkaline trachytes, the rhyolites are depleted in zirconium (Fig. 11) but zircon is absent from these lavas. They contain F-rich arfvedsonite (up to 4.6 wt% fluorine), and F-rich fluids can control Zr distribution, as shown by Pearce and Norry (1979). Their relatively low LREE contents compared to those of other Benue felsic lavas, the negative europium anomaly, and the relatively high HREE contents (Fig. 13b) cannot readily be explained by any fractional crystallisation process from basaltic or trachytic magmas. These features are common for rhyolites from alkaline series (Azambre et al. 1992) and, if they remain unexplained in many cases, high (even extreme) enrichment in HREEs may be the result of F-rich vapour-phase crystallisation, as proposed for peraluminous rhyolites of Trans-Pecos in a continental arc setting (Price et al. 1990).

Geophysical data (Stuart et al. 1985) indicate abnormally thin continental crust (23 km), and low seismic wave velocities (6 km/s) can be an argument in favour of a partially melted crust beneath the Upper Benue valley Cretaceous sandstones. Nevertheless, the existence of good correlations in binary diagrams (Rb–Th, Yb and Nb, Fig. 11) does not support the formation of the rhyolite magma by partial melting of the Pan-African continental crust. The Pan-African continental crust exposed to the north and south of the Upper Benue valley is composed of a metamorphic basement intruded by mafic to intermediate plutonic bodies of calc-alkaline affinity, with a typical Nb trough in primitive mantle-normalised diagrams (Fig. 14). Geochemical data of one gneiss from this basement (sample IN4, Table 3) are similar in SiO_2 , TiO_2 , Al_2O_3 , MgO, CaO, and P_2O_5 but they are richer in Sr and Ba, and poorer in Rb, Th, REEs (except Eu), Zr and, above all, Nb, when compared to the Upper Benue valley rhyolites. The dissimilarity between

(La/Sm)_N, Zr/Nb and Rb/La values in the rhyolite (sample F3: 8.1, 1.7 and 6.2 respectively) and the upper crust materials (IN4: 2.7, 15.4 and 9.2 respectively) suggests that the rhyolite is not derived from the upper continental crust by a partial melting process. Its genesis is probably dependent upon volatile- and halogen-rich fluids, as attested by the occurrence of F-rich minerals, calcite and analcite in these rhyolites, and these fluids could be derived from a metasomatised mantle source (e.g. Dautria et al. 1992; Hauri et al. 1993; Rudnick et al. 1993, McDonough and Rudnick 1998). The nearby occurrence in the same Upper Benue valley (at Tchircotché) of carbonated lamprophyres (monchiquites) supports the presence of a fluid-rich mantle source. These fluids have interacted with the upper continental crust, resulting in the high Sr_i (0.7107) and a low ε Nd_(37 Ma) value (+0.4) measured in the rhyolites when compared to basalts and phonolite (Table 4).

Crustal contamination

Xenocrysts of quartz occur in basaltic lavas, mugearites and trachytes (up to 6.5 vol%). These quartz xenocrysts presumably come from the Upper Benue valley sandstones. A magmatic origin has been suggested for the quartz on the basis of their fluid inclusions (Clochiatti, personal communication 1991). Although CO₂ inclusions predominate in number, they appear contemporaneous with aqueous inclusions. CO₂ inclusions have a centripetal distribution inside the quartz crystals. The quartz grains of the Upper Benue valley sandstones derive from the plutonic and metamorphic rocks of the basement which have been eroded during Cretaceous times. Quartz crystals occur in trachytes and rhyolites whereas these lavas plot in the sanidine field, far from the cotectic line in a Q–Ab–Or diagram (Fig. 15), implying that quartz cannot have crystallised in such magmas and therefore that those quartz crystals are inherited from the surrounding sandstones. In fact, the assimilation of quartz only modifies the silica contents of the lavas.

All the Upper Benue valley, felsic lavas (except some biotite-bearing trachytes) exhibit high positive Zr anomalies (Fig. 14). Similar anomalies have been reported for other felsic lavas from Cameroon (Tchabal Nganha volcano: Nono et al. 1994; Kapsiki plateau: Ngounouno et al. 2000) as well as for nepheline syenites from the Kokoumi anorogenic complex (Ngounouno et al. 2001) in the Upper Benue valley. The Zr enrichment (755 to 1,185 ppm) in the Upper Benue valley felsic lavas which lack zircon phenocrysts can readily be explained by the fact that zircon crystallisation is inhibited in peralkaline liquids (Watson 1979). These high Zr abundances are not related to bulk assimilation of partially melted crustal materials by the magmas from which these felsic lavas derived, as crustal materials are characterised by rather low Zr contents (sample IN4: 63 ppm Zr; Fig. 14).

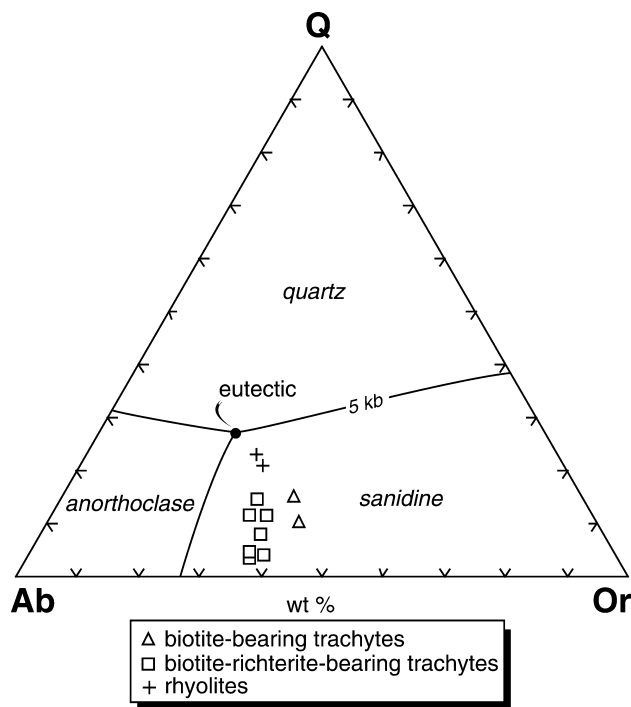


Fig. 15 Plots of normative Q, Or, and Ab compositions for trachytes and rhyolites of the Upper Benue valley with 5-kbar curves (after Carmichael et al. 1974) for water-saturated liquids in equilibrium with quartz and alkali feldspars

The initial (at 37 Ma) Sr_i isotopic compositions increase in the sequence basalt (0.7034)–mugearite (0.7048)–trachyte (0.7066 to 0.7106)–rhyolite (0.7107) (Fig. 16). These data define a trend of increasing Sr_i with increasing SiO₂ contents which suggests a progressive crustal contamination during magmatic evolution, the crustal influence being strongly marked for lavas with

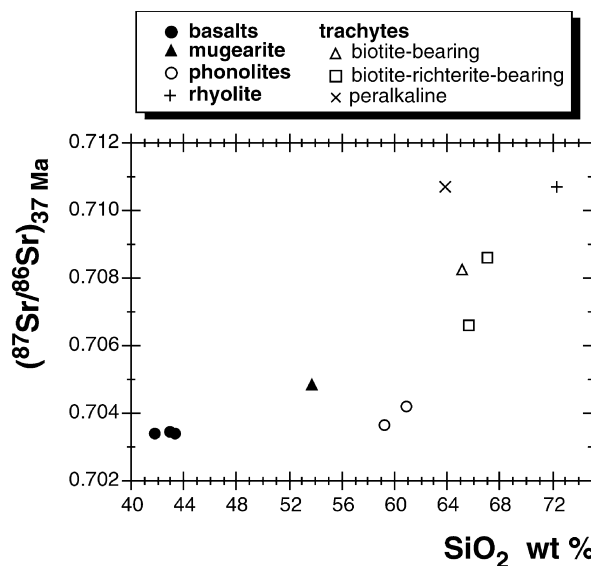


Fig. 16 Plot of the initial (at 37 Ma) Sr isotopic composition versus SiO₂ content (wt%) for Upper Benue valley lavas

more than 62 wt% SiO₂. AFC modelling (after De Paolo 1981), using partition coefficients from Mahood and Stimač (1990) and a Pan-African gneiss country rock (sample IN4: Sr = 112 ppm; (⁸⁷Sr/⁸⁶Sr)_{37 Ma} = 0.749; Table 4) as a contaminant, has been attempted. The differentiation from biotite-richterite-bearing trachytes to peralkaline trachytes (or to rhyolite) requires a Ma/Mc ratio of 0.1 and a fractionation process (F ≈ 0.9) involving only feldspar to comply with the (⁸⁷Sr/⁸⁶Sr)_{37 Ma} values (≈ 0.710) of the considered lavas.

Conclusions

The genesis of the alkaline lava series of the Upper Benue valley probably began with the segregation of primary magmas of basaltic composition within the intralithospheric peridotite mantle which has a HIMU-type geochemical signature. The trace-element and Sr and Nd isotopic composition of the primary magma is the same as those of other magmas from which basalts were generated all along the Cameroon Line, in both continental and oceanic sectors. These primary magma ponded in infra-crustal reservoirs where they inherited olivine (≈ Fo₉₀) and spinel xenocrysts. The basalts derived from these magmas through crystal fractionation of olivine, clinopyroxene and Fe–Ti oxides. The mugearites have a hybrid origin resulting from mixing between basaltic and felsic magmas. Most basaltic magma batches have been involved in such mixing processes, as attested by the relatively high volume of mugearites compared to that of basalts. The phonolites have roughly the same (or slightly more evolved) Sr- and Nd-isotope signatures as the basalts. They presumably derived through further crystal fractionation of amphibole ± aegirine-augite ± sphene ± apatite. The trachytes were probably generated by the same process followed by protracted fractionation of apatite ± biotite ± alkali-feldspar and concomitant contamination by assimilation of crustal-derived fluids. The rhyolites are probably derived from peralkaline trachyte magmas contaminated by crustal components through assimilation–fractional crystallisation. Fluids from deep mantle origin also played a significant role in the genesis of the felsic lavas, as attested by the presence of carbonates, F-rich biotite and arfvedsonite.

Acknowledgements The French Ministère de la Coopération is acknowledged for providing grants to I.N. for stays in France in the Laboratoire de Magmatologie et de Géochimie Inorganique et Expérimentale, Université Pierre et Marie Curie, Paris, and for financially supporting the research work. This work is part of a Thèse de l'Université Pierre et Marie Curie (Paris VI) by I.N. Fieldwork (B.D. and I.N.) was substantially supported by the Faculty of Sciences of the University of Yaoundé (Dean, Prof. G. Valet). The isotopic measurements in the Université Libre de Bruxelles were financially supported by the Ministère des Affaires Économiques (projet SGB/NAT 91-98). The constructive comments of J. Keller and an anonymous reviewer are greatly appreciated.

References

- Ashwal LD, Demaiffe D, Torsvik, TH (2002) Petrogenesis of Neoproterozoic granitoids and related rocks from the Seychelles: the case for an Andean-type arc origin. *J Petrol* 43:45–83
- Azambre B, Rossy M, Albarède F (1992) Petrology of the alkaline magmatism from the Cretaceous North-Pyrenean Rift Zone (France and Spain). *Eur J Mineral* 4:813–834
- Ballentine CJ, Lee D-C, Halliday AN (1997) Hafnium isotopic studies of the Cameroon line and new HIMU paradoxes. *Chem Geol* 139:111–124
- Barth TFW (1963) The composition of nepheline. *Schweiz Mineral Petrol Mitt* 43:153–164
- Benkhelil J (1988) Structure et évolution géodynamique du bassin intracontinental de la Bénoué (Nigeria). *Bull Centre Rech Explor Prod Elf-Aquitaine* 12:29–128
- Bonhomme M, Thuizat R, Pinault Y, Clauer N, Wendling A, Winkler R (1975) Méthode de datation potassium-argon. Appareillage et technique. *Notes Techn Inst Géol Univ Louis Pasteur Strasbourg* 3:1–53
- Bonnefoi CC, Provost A, Albarède F (1995) The 'Daly gap' as a magmatic catastrophe. *Nature* 378:270–272
- Carignan J, Hild P, Mévelle G, Morel J, Yeghicheyan D (2001) Routine analyses of trace elements in geological samples using flow injection and low pressure on-line liquid chromatography coupled to ICPMS: a study of geochemical reference materials BR, DR-N, UB-N, AN-G and GH. *Geostand Newslett* 25:187–198
- Carmichael ISE, Turner FJ, Verhoogen J (1974) *Igneous petrology*. McGraw-Hill, New York, pp 1–739
- Charles RW (1975) The phase equilibrium of richterite and ferro-richterite. *Am Mineral* 60:367–374
- Cox A, Dalrymple GB (1967) Statistical analysis of geomagnetic reversal data and the precision of potassium-argon dating. *J Geophys Res* 72:2603–2614
- Creaser RA, Price RC, Wormald RJ (1991) A-type granites revisited: assessment of a residual-source. *Geology* 19:163–166
- Dautria JM, Dupuy C, Takherist D, Dostal J (1992) Carbonate metasomatism in the lithospheric mantle: peridotitic xenoliths from a mellitic district of the Sahara basin. *Contrib Mineral Petrol* 111:37–52
- DePaolo DJ (1981) Trace element and isotopic effects of combined wallrock assimilation and fractional crystallization. *Earth Planet Sci Lett* 53:189–202
- Déruelle B, N'ni J, Kambou R (1987) Mont Cameroon, an active volcano of the Cameroon Line. *J Afr Earth Sci* 6:197–214
- Déruelle B, Moreau C, Nkoumbou C, Kambou R, Lissom J, Njongfang E, Ghogomu RT, Nono A (1991) The Cameroon Line: a review. In: Kampunzu AB, Lubala RT (eds) *Magmatism in extensional structural settings. The Phanerozoic African Plate*. Springer, Berlin Heidelberg New York, pp 274–327
- Déruelle B, Ngounouno I, Nkoumbou C (1998) Mt Cameroon, Mt Etinde, and Bioko Island volcanoes of the "Cameroon hot Line". In: *Program Abstr Vol Conf Evolution of Ocean Island Volcanoes, Galapagos Islands, 4–12 June. Penrose Conf Ser*, p 28
- Déruelle B, Bardintzeff J-M, Cheminée J-L, Ngounouno I, Lissom J, Nkoumbou C, Etame J, Hell JV, Tanyileke G, N'ni J, Bekoa A, Ntomu N, Nono A, Wandji P, Fosso J, Nkouathio DG (2000) Eruptions simultanées de basalte alcalin et de hawaïite au Mont Cameroun (28 mars–17 avril 1999). *C R Acad Sci Paris Sér IIA Earth Planet Sci* 331:525–531
- Draper DS (1991) Late Cenozoic bimodal magmatism in the northern Basin and Range Province of southeastern Oregon. *J Volcanol Geotherm Res* 47:299–328
- Duggan MB (1988) Zirconium-rich sodic pyroxenes in felsic volcanics from the Warrumbungle Volcano, Central New South Wales. *Mineral Mag* 52:491–496
- Duncan R (1981) Hotspots in the southern oceans – an absolute frame of reference for motion of the Gondwana continents. *Tectonophysics* 74:29–42

- Ernst WG (1962) Synthesis, stability relations and occurrence of riebeckite-arfvedsonite solid solutions. *J Geol* 70:689–736
- Esperança S, Holloway JR (1987) On the origin of some mica lamprophyres: experimental evidence from a mafic minette. *Contrib Mineral Petrol* 95:207–216
- Ezangono J, Déruelle B, Ménard J-J (1995) Benmoreites from Tchabal Djinga volcano (Adamawa, Cameroon): products of kaersutite + plagioclase assimilation by a trachytic magma. *Terra AbstrSuppl Terra Nova* 5:1:161
- Farges F, Brown GE Jr, Velde D (1994) Structural environment of Zr in two inosilicates from Cameroon: mineralogical and geochemical implications. *Am Mineral* 79:838–847
- Ferguson AK (1977) The natural occurrence of aegirine–neptunite solid solution. *Contrib Mineral Petrol* 60:247–253
- Fitton JG (1980) The Benue trough and Cameroon line – a migration rift system in West Africa. *Earth Planet Sci Lett* 51:132–138
- Fitton JG (1983) Active versus passive continental rifting: evidence from the West African rift system. *Tectonophysics* 94:473–481
- Fitton JG (1987) The Cameroon line, West Africa: a comparison between oceanic and continental alkaline volcanism. In: Fitton JG, Upton BGD (eds) *Alkaline igneous rocks*. *Geol Soc Lond Spec Publ* 30:273–291
- Gèze B (1943) Géographie physique et géologie du Cameroun Occidental. *Mém Mus Hist Nat Nouv Sér* 17:1–272
- Giret A, Bonin B, Léger J-M (1980) Amphibole compositional trends in oversaturated and undersaturated alkaline plutonic ring-complexes. *Can Mineral* 18:481–495
- Grant NK, Rex DC, Freeth SJ (1972) Potassium-argon ages and strontium isotope ratio measurements from volcanic rocks in northeastern Nigeria. *Contrib Mineral Petrol* 69:97–103
- Guiraud R (1993) Late Jurassic-Early Cretaceous rifting and Late Cretaceous transpressional inversion in the Upper Benue basin (NE Nigeria). *Bull Centre Rech Explor Prod Elf-Aquitaine* 17:371–383
- Guiraud R, Bosworth W (1997) Senonian basin inversion and rejuvenation of rifting in Africa and Arabia: synthesis and implications to plate-scale tectonics. *Tectonophysics* 282:39–82
- Halliday AN, Dickin AP, Fallick AE, Fitton JG (1988) Mantle dynamics: a Nd, Sr, Pb and O isotopic study of the Cameroon line volcanic chain. *J Petrol* 29:181–211
- Hamilton DL (1961) Nephelines as crystallization temperature indicators. *J Geol* 22:433–466
- Hansen K (1980) Lamprophyres and carbonatitic lamprophyres related to rifting in the Labrador Sea. *Lithos* 13:145–153
- Hauri EH, Shimizu N, Dieu JJ, Hart SR (1993) Evidence for hotspot-related carbonatite metasomatism in the oceanic upper mantle. *Nature* 365:221–227
- Hofmann AW (1988) Chemical differentiation of the Earth: the relationship between mantle, continental crust, oceanic crust. *Earth Planet Sci Lett* 90:297–314
- Kampunzu AB, Popoff M (1991) Distribution of the main Phanerozoic African rifts and associated magmatism: introductory notes. In: Kampunzu AB, Lubala RT (eds) *Magmatism in extensional structural settings. The Phanerozoic African Plate*. Springer, Berlin Heidelberg New York, pp 2–10
- Larsen LM (1977) Aenigmatite from the Ilimaussaq intrusion, south Greenland: chemistry and petrological implications. *Lithos* 10:257–270
- Leake BE et al. (1997) Nomenclature of amphiboles: report of the subcommittee on amphiboles of the International Mineralogical Association Commission on new minerals and mineral names. *Mineral Mag* 61:295–321
- Leeman WP (1978) Distribution of Mg between olivine and silicate melt and its complications regarding melt structure. *Geochim Cosmochim Acta* 42:789–800
- Lightfoot PC, Hawkesworth CJ, Sethna SF (1987) Petrogenesis of rhyolites and trachytes from the Deccan Trap: Sr, Nd and Pb isotope and trace element evidence. *Contrib Mineral Petrol* 95:44–54
- MacDonald R (1987) Quaternary peralkaline silicic rocks and caldera volcanoes of Kenya. In: Fitton JG, Upton BGD (eds) *Alkaline igneous rocks*. *Geol Soc Lond Spec Publ* 30:313–333
- Mahood GA, Stimac JA (1990) Trace-element partitioning in pantellerites and trachytes. *Geochim Cosmochim Acta* 54:2257–2276
- Marsh JS (1975) Aenigmatite stability in silica-undersaturated rocks. *Contrib Mineral Petrol* 50:135–144
- Marzoli A, Renne PR, Piccirillo EM, Francesca C, Bellieni G, Melfi AJ, Nyobe JB, N'ni J (1999) Silicic magmas from the continental Cameroon Volcanic Line (Oku, Bambouto and Ngaoundere): ^{40}Ar - ^{39}Ar dates, petrology, Sr-Nd-O isotopes and their petrogenetic significance. *Contrib Mineral Petrol* 135:133–150
- Marzoli A, Piccirillo EM, Renne PR, Bellieni G, Lacumin M, Nyobe JB, Tongwa AT (2000) The Cameroon Volcanic Line revisited: petrogenesis of continental basaltic magmas from lithospheric and asthenospheric mantle sources. *J Petrol* 41:87–109
- McDonough WF, Rudnick RL (1998) Mineralogy and composition of the upper mantle. In: Hemley RJ (ed) *Ultrahigh-pressure mineralogy: physics and chemistry of the Earth's deep interior*. *Mineral Soc Am Rev Mineral* 37:139–175
- Meyers JB, Rosendahl BR, Harrison CGA, Ding Z-A (1998) Deep-imaging seismic and gravity results from the offshore Cameroon Volcanic Line, and speculation of African hotlines. *Tectonophysics* 284:31–63
- Montigny R, Le Mer O, Thuizat R, Whitechurch H (1988) K–Ar and ^{40}Ar - ^{39}Ar study of metamorphic rocks associated with the Oman ophiolite: tectonic implications. *Tectonophysics* 151:341–362
- Moreau C, Regnault J-M, Déruelle B, Robineau B (1987) A new tectonic model for the Cameroon Line, Central Africa. *Tectonophysics* 139:317–334
- Morgan WJ (1983) Hotspot tracks and the early rifting of the Atlantic. *Tectonophysics* 94:123–139
- Morimoto N (1989) Nomenclature of pyroxenes. *Can Mineral* 27:143–156
- Mysen OB (1991) Volatiles in magmatic liquids. In: Perchuk LL (ed) *Progress in metamorphic and magmatic petrology: a memorial volume in honor of D.S. Korzhinskii*. University Press, Cambridge, pp 435–475
- Ngounouno I (1993) *Pétrologie du magmatisme cénozoïque de la vallée de la Bénoué et du plateau Kapsiki (nord du Cameroun)*. Thèse Doct Université Pierre et Marie Curie, Paris, pp 1–280
- Ngounouno I, Nkoumbou C, Loulé J-P (1997) Relations entre l'évolution tectono-sédimentaire et le magmatisme du bassin de Garoua (nord du Cameroun). *Afr Geosci Rev* 4:451–460
- Ngounouno I, Déruelle B, Demaiffe D (2000) Petrology of the bimodal Cenozoic volcanism of the Kapsiki Plateau (northernmost Cameroon, Central Africa). *J Volcanol Geotherm Res* 102:21–44
- Ngounouno I, Moreau C, Déruelle B, Demaiffe D, Montigny R (2001) *Pétrologie du complexe alcalin sous-saturé de Kokoumi (nord du Cameroun)*. *Bull Soc Géol Fr* 172:675–686
- Nielsen TFD (1979) The occurrence and formation of Ti-aegirines in peralkaline syenites. An example from the Tertiary ultramafic alkaline Gardiner complex, East Greenland. *Contrib Mineral Petrol* 69:235–244
- Nimis P (1999) Clinopyroxene geobarometry of magmatic rocks. Part 2. Structural geobarometers for basic to acid tholeiitic and mildly alkaline magmatic systems. *Contrib Mineral Petrol* 135:62–74
- Nono A, Déruelle B, Demaiffe D, Kambou R (1994) Tchabal Nganha volcano in Adamawa (Cameroon): petrology of a continental alkaline lava series. *J Volcanol Geotherm Res* 60:147–178
- Pearce JA, Norry MJ (1979) Petrogenetic implications of Ti, Zr, Y, and Nb variations in volcanic rocks. *Contrib Mineral Petrol* 69:33–47

- Poudjom Djomani YH, Nnange JM, Diament M, Ebinger GJ, Fairhead JD (1995) Effective elastic thickness and crustal thickness variations in West-Central Africa inferred from gravity data. *J Geophys Res* 100:22047–22070
- Poudjom Djomani YH, Diament M, Wilson M (1997) Lithospheric structure across the Adamawa plateau (Cameroon) from gravity studies. *Tectonophysics* 273:317–327
- Presnall DC, Dixon SA, Dixon JR, O'Donnel TH, Brenner NL, Srook RL, Dycus DW (1978) Liquidus phase relations on the join diopside–forsterite–anorthite from 1 atm to 20 kb: their bearing on the generation and crystallization of basaltic magma. *Contrib Mineral Petrol* 66:203–220
- Price JG, Rubin JN, Henry CD, Pinkston TL, Tweedy SW, Koppelaar DW (1990) Rare-metal enriched peraluminous rhyolites in a continental arc, Sierra Blanca area, Trans-Pecos Texas; chemical modification by vapor-phase crystallization. In: Stein HJ, Hannah JL (eds) *Ore-bearing granite systems; petrogenesis and mineralizing processes*. *Geol Soc Am Spec Pap* 246:103–120
- Roeder PL, Emslie RF (1970) Olivine–liquid equilibrium. *Contrib Mineral Petrol* 29:275–289
- Rudnick RL, McDonough, WF Chappell BW (1993) Carbonatite metasomatism in the northern Tanzanian mantle: petrographic and geochemical characteristics. *Earth Planet Sci Lett* 114:463–475
- Steiger RH, Jäger E (1977) Subcommittee of geochronology: convention on the use of decay constants in geo- and cosmochronology. *Earth Planet Sci Lett* 36:359–362
- Stormer Jr C (1983) The effects of recalculation on estimates of temperature and oxygen fugacity from analyses of multicomponent iron-titanium oxides. *Am Mineral* 68:586–594
- Strong DF, Taylor RP (1984) Magmatic-subsolidus and oxidation trends in composition of amphiboles from silica-saturated peralkaline igneous rocks. *Tschermaks Mineral Petrogr Mitt* 32:211–222
- Stuart GW, Fairhead JD, Dorbath L, Dorbath C (1985) A seismic refraction study of the crustal structure associated with the Adamawa Plateau and Garoua Rift, Cameroon, West Africa. *Geophys J R Astron Soc* 81:1–12
- Thompson GM, Smith IEM, Malpas JG (2001) Origin of oceanic phonolites by crystal fractionation and the problem of the Daly gap: an example from Rarotonga. *Contrib Mineral Petrol* 142:336–346
- Thornton CP, Tuttle OF (1960) Chemistry of igneous rocks. I. Differentiation index. *Am J Sci* 258:664–684
- Van Houten FB (1983) Sirte Basin, northcentral Libya: Cretaceous rifting above a fixed mantle hotspot? *Geology* 11:115–118
- Watson EB (1979) Zircon saturation in felsic liquids: experimental results and applications to trace element geochemistry. *Contrib Mineral Petrol* 70:407–419
- Wellman TR (1970) The stability of sodalite in a synthetic syenite plus aqueous chloride fluid system. *J Petrol* 11:149–171